BMC Endocrine Disorders

CASE REPORT

Open Access

Flow cytometry immune profiling of recurrent and newly diagnosed growth hormone secreting pituitary neuroendocrine tumors: comparison of two clinical cases

Daria Lisina[1], Valeria Mazeeva[1], Elena Zakharova[1], Alyona Sorokina[1], Lilya Dzhemileva[1], Andrey Grigoriev[1], Vilen Azizyan[1], Alexandra Shutova[1], Ekaterina Pigarova[1], Larisa Dzeranova[1], Galina Melnichenko[1], Sergei Rumiantsev[1], Natalia Mokrysheva[1], Vladimir Chekhonin[1] and Marina Loguinova[1*]

Abstract

Early detection of aggressive pituitary neuroendocrine tumors (PitNETs) remains challenging due to the absence of reliable markers that can predict disease progression. Aggressive tumors are typically identified through long-term observation. Tumor immune microenvironment (TIME) is crucial for understanding PitNETs' heterogeneity and identifying potential predictors of tumor aggressiveness. In this study, we analyzed immune profile of micro- and macroenvironment in two somatotropinomas (aggressive and non-aggressive) using flow cytometry. We observed lymphopenia and elevated neutrophil levels in the periphery in the patient with tumor recurrence. The aggressive TIME showed greater leukocyte infiltration, with lymphoid cells predominating over myeloid cells along with a higher proportion of CD4 + T cells over CD8 + T cells. We detected double-positive CD4 + CD8 + population, high level of regulatory T cells and a sharp increase in PD-1 + expressing T cells over six months during recurrence. In the blood of the patient with tumor recurrence, we observed reduced granule-mediated cytotoxicity of CD8 + T cells and NK-cells. In the aggressive TIME the number of effector cells producing perforin and granzyme B—both independently and simultaneously was significantly lower. The proportion of CD3-CD20- NK cells and CD3-CD56 + NK cells was low after the first recurrence but increased sharply after six months. The ratio of monocyte subpopulations in tumor differed from that in blood, with CD16 + expressing monocytes predominating in the TIME of both patients. M2 macrophages in TIME rose sharply to 60.8% over six months during recurrence. In several immunological parameters, the patient with tumor recurrence exhibited a more pronounced immunosuppressive profile.

Keywords Aggressive pituitary neuroendocrine tumors, PitNETs, Somatotropinoma, Immune microenvironment, Flow cytometry

Introduction

Neuroendocrine pituitary tumors (PitNETs) represent one of the most common brain tumors, accounting for approximately 10–15% of all primary intracranial tumors [1]. While most PitNETs are considered benign and slow-growing, 0.13–0.4% of cases exhibit craniospinal dissemination or systemic metastases, classifying them as true pituitary carcinomas [2]. Moreover, some

*Correspondence:
Marina Loguinova
marina.loguinova@mail.ru
[1] Endocrinology Research Centre, Moscow 117036, Russia

tumors demonstrate an aggressive clinical behavior with frequent complications arising from both tumor growth and hormonal hypersecretion [3]. Despite numerous efforts to establish clear classification criteria for these aggressive tumors, no standardized definition or criteria currently exist. The most widely accepted definition describes these tumors as invasive and rapidly growing, with frequent recurrences and resistance to conventional treatments such as neurosurgery, pharmacotherapy, and radiation therapy [4]. The precise incidence of aggressive PitNETs remains unclear, largely due to the lack of a unified definition and clear clinical or immunohistochemical characteristics [5]. On average, up to 35% of PitNETs are invasive, infiltrating nearby structures such as the cavernous sinuses, bones, sphenoid sinuses, and nerve sheaths. Approximately 10% of these tumors demonstrate aggressive behavior and resistance to standard therapies [6, 7].

From a histological perspective, aggressive PitNETs exhibit characteristics associated with increased proliferation, such as a Ki-67 index greater than 3%, elevated mitotic activity, and p53 expression [8]. However, the presence of these markers does not reliably predict tumor aggressiveness, and their prognostic value remains controversial. Consequently, the latest WHO classification does not provide threshold values for these markers or propose a quantitative assessment approach. Currently, prognostic stratification is limited to specific tumor types and subtypes, including immature PIT1 lineage tumors, Crooke cell tumors, null-cell tumors, and biochemically non-functioning "silent" corticotropic tumors, which are considered more aggressive [2, 9].

Invasive PitNETs often have an irregular shape, especially after subtotal resection when complete removal is not possible, making it challenging to assess progressive growth [10]. Currently, there are no standardized radiographic criteria for evaluating treatment response in these tumors. Existing imaging techniques, designed for spherical intracranial tumors, may be suboptimal for assessing PitNETs. Although the use of RECIST criteria—commonly applied in oncology—has been proposed to evaluate tumor progression, but still, there is no consensus on what constitutes clinically significant tumor growth or an unusually high growth rate [11]. Despite extensive research on aggressive PitNETs, no definitive morphological or histological marker has been identified that reliably predicts tumor aggressiveness [12]. Some studies suggest a correlation between tumor aggressiveness and the expression of estrogen receptors [13], epidermal growth factor receptors (EGFR) [14], fibroblast growth factors (FGF) and their receptors (FGFR) [15], bromodomain-containing protein 4 (BRD4) [16], as well as decreased expression of MSH6/MSH2 proteins involved in DNA repair [17]. However, further investigation is needed to confirm these associations.

The treatment of aggressive PitNETs requires a multimodal approach, including neurosurgery, radiation therapy, and pharmacotherapy. But even this approach leaves treatment ineffective for 10–50% of patients, depending on the hormonal type of the PitNET. Non-conventional treatments such as chemotherapeutic agents or peptide receptor radionuclide therapy have highly limited use in PitNETs and often not very effective forcing the search for new approaches to the treatment of these tumors [18–23].

Tumor cells often overexpress immune checkpoint ligands such as programmed cell death protein ligand 1 (PD-L1), membrane proteins CD80 and CD86, or produce factors that upregulate immune checkpoints (e.g., PD-1, CTLA-4, LAG3) on immune cells, thereby suppressing the immune system's cytotoxic response. Expression of these immune checkpoint ligands has been observed in various types of adenomas [24], which may contribute to chemotherapy resistance [25]. Immune checkpoint inhibitors have shown potential for treating aggressive PitNETs, including ipilimumab (a monoclonal antibody against CTLA-4) in combination with nivolumab and pembrolizumab (PD-1/PD-L1 inhibitors) [26]. Therefore, immune checkpoint inhibitors represent a promising potential therapy for aggressive pituitary tumors, though further study of the tumor microenvironment is required since it has been little studied to date [24].

Characterizing the tumor immune microenvironment (TIME) of PitNETs could provide crucial insights for tumor prognosis and immunotherapy efficacy. Tumor development is closely influenced by its microenvironment, which includes stromal and immunocompetent cells, blood vessels, extracellular matrix, and various regulatory molecules such as cytokines, chemokines, and growth factors [27]. As tumors evolve, they modify TIME to become immunosuppressive, allowing them to evade immune surveillance [28]. Research of PitNETs is increasingly focused on TIME to stratify patients based on types, number and localization of infiltrating cells, as this may guide treatment decisions and inform prognosis [29]. TIME has been linked to PitNET aggressiveness, abnormal hormone secretion, tumor size, invasion, progression, recurrence, and treatment response [24]. However, the clinical significance of TIME in PitNETs remains unclear [30].

Somatotropinomas, a subtype of PitNETs, are typically characterized by high levels of tumor-infiltrating lymphocytes (TILs) and tumor-associated macrophages (TAMs) [31]. Larger adenomas have been found to contain greater numbers of both macrophages and lymphocytes [32]. In somatotropinomas with cavernous sinus

invasion, the number of CD8 + T cells is significantly lower [33]. On the other hand, a positive correlation has been observed between CD8 + T cells and the expression of matrix metalloproteinase-9 (MMP-9), a biomarker of tumor invasiveness [34].

Increasing evidence suggests that describing cancer progression solely in terms of tumor cells is insufficient. Tumor progression is now understood as a dynamic interplay between invasive tumor cells and the immune system, with tumors often evading immune surveillance in the later stages of development. An international consortium has proposed expanding the current American Joint Committee on Cancer (AJCC) guidelines for determining tumor stage. This expanded model would incorporate immunological parameters into the traditional TNM system (T—tumor size, N—lymph node involvement, M—metastasis), introducing the so-called Immunoscore [35]. Indeed, the clinical outcome of cancer can vary significantly among patients with the same tumor stage, as the tumor phenotype is influenced not only by tumor cells but also by other components of the tumor microenvironment, including immune cells.

In this paper, we compare the TIME of two somatotropinomas. One case involved a newly diagnosed GH-secreting pituitary microadenoma in a patient with confirmed active acromegaly, while the other was a recurrence of a supra-, infra-, retro-, and laterosellar GH-secreting pituitary macroadenoma (S-Knosp IV, D-Knosp I) in a patient who had previously undergone transnasal transsphenoidal surgery and achieved remission of acromegaly. Additionally, we analyzed the composition of lymphocyte and myeloid cell subpopulations in the blood of these patients to assess systemic immunity. Multicolor flow cytometry was employed, using a protocol we previously developed, to quantify the relative proportions of multiple cell subpopulations. Our study revealed significant differences in the macro- and microenvironment of the GH-secreting PitNETs, one of which was clearly aggressive. These differences may underlie the varying courses of tumor aggressiveness. However, identifying the key immunological parameters that could serve as biomarkers for potential recurrence will require analysis of a larger cohort of somatotropinomas. Our findings provide a foundation for more comprehensive studies on the role of the immune system—both systemically and locally—in controlling PitNETs progression and identifying immune predictors of tumor aggressiveness.

Patients and methods

Patients

The diagnosis of acromegaly and hormonal activity of pituitary adenomas in the patients were established through a comprehensive examination at the Endocrinology Research Centre, Moscow, Russian Federation. This included the collection of complaints, life and family history, a systematic physical examination, and both laboratory (including hormonal blood analysis) and instrumental studies (brain MRI with contrast, computer perimetry and ophthalmoscopy). Prolactin, growth hormone (GH), and insulin-like growth factor 1 (IGF-1) levels were measured using the automated Liaison system (DiaSorin, Italy). MRI with gadolinium contrast enhancement was performed on a high-field General Electric 450W magnetic resonance scanner with a power of 1.5 T. Transnasal transsphenoidal adenomectomy was performed in accordance with clinical guidelines for neurosurgical treatment of patients with pituitary adenomas after obtaining written informed consent.

The morphological analysis included both histological and immunohistochemical (IHC) methods, evaluating the tumor's staining properties, structure, and the presence of hemorrhage, necrosis, fibrosis, and mitotic figures. The IHC study used antibodies to synaptophysin, low-molecular-weight cytokeratin CAM5.2, tropic hormones (prolactin, GH), and somatostatin receptor subtypes 2 and 5 (SSTR2, SSTR5), as well as the cell proliferation marker Ki-67.

Case description 1

In 2021, patient P., a 63-year-old female, was diagnosed with acromegaly during an examination due to complaints of enlarged facial features, increased foot size by two shoe sizes, severe sweating, and knee joint pain. An elevated IGF-1 level and a pituitary endosellar microadenoma were detected, but no neurosurgical treatment or drug therapy was prescribed at that time. The patient also had complications of acromegaly, including diabetes mellitus, arterial hypertension, acromegalic cardiopathy, and a multinodular colloid euthyroid goiter (Bethesda II). In October 2022, she suffered a cryptogenic ischemic stroke with hemorrhagic transformation in the left middle cerebral artery (MCA) basin, which led to complications, including central paresis of the VII cranial nerve, dysarthria, and mild right-sided hemiparesis. In December 2022, her IGF-1 level was 719.8 ng/ml (age-specific reference range: 17–238 ng/ml). An MRI of the pituitary gland with contrast in April 2023 confirmed an endosellar microadenoma on the right side of the sella turcica, measuring 9.3×7.4×6.8 mm, deforming the medial wall of the cavernous sinus. By September 2023, her hormonal blood tests confirmed an active stage of acromegaly with an elevated IGF-1 level of 1185 ng/ml, and MRI showed a slight increase in adenoma size to 9.5×7.5×8 mm. A clinical blood test also revealed a slight decrease in monocytes (Table S1).

In September 2023, the patient underwent transnasal transsphenoidal adenomectomy. However, postoperative testing revealed no suppression of GH to less than 1 ng/ml during the oral glucose tolerance test (OGTT) on the 7th day, which is an unfavorable prognostic sign indicating a lack of disease remission [36]. Morphological examination confirmed a solid pituitary tumor consisting of chromophobic cells with oxyphilic cytoplasm; no mitotic figures were observed in 10 high-power fields. IHC analysis revealed densely granulated somatotroph neuroendocrine tumor markers, including synaptophysin expression and uneven cytoplasmic staining in up to 80% of cells for GH and CAM5.2, with no prolactin detected. Moderate expression of somatostatin receptor subtypes 2 (IRS 8) and 5 (IRS 6) was present in over 80% of tumor cells, and the Ki-67 labeling index was 3.0%.

During a follow-up examination 12 months after surgical treatment, remission of acromegaly was confirmed, with an IGF-1 level of 99.2 ng/ml. Brain MRI with contrast enhancement showed no evidence of pituitary neuroendocrine tumor recurrence – Fig. 1. The clinical blood test results remained within the reference ranges. (Table S1).

Case description 2

Patient R. first noted a menstrual cycle disorder such as amenorrhea, episodic headaches and decreased visual acuity in the left eye, gradual weight gain of 10 kg over the course of a year at the age of 18 years (in 2021). In February 2022, following ineffective treatment with dydrogesterone prescribed by a gynecologist, hyperprolactinemia was detected with prolactin levels reaching 2746.6 mIU/l (reference range: 94–557 mIU/l). An MRI with contrast revealed a pituitary lesion measuring 41×25x18 mm, extending into the left cavernous sinus (Knosp IV), the third ventricle, deforming the sphenoid sinus, and compressing the optic chiasm. Cabergoline therapy was initiated at a dose of 0.5 mg twice a week, leading to a reduction in prolactin levels to 921.6 mIU/l by April 2022, with biologically active (monomeric) prolactin at 870 mIU/l (reference range: 64–365 mIU/l). Elevated IGF-1 levels at 619.1 ng/ml (reference range: 94–479 ng/ml) and the absence of GH suppression during OGTT confirmed the active stage of acromegaly, even in the absence of characteristic facial changes. The patient was also diagnosed with partial atrophy and optic neuropathy of both optic nerves, right-sided hemianopsia, and secondary hypothyroidism, for which sodium levothyroxine therapy was prescribed.

In May 2022, the patient underwent transnasal transsphenoidal adenomectomy. Postoperatively, visual acuity improved, and headaches became less frequent and less intense. Morphological examination revealed an eosinophilic pituitary tumor with a solid-trabecular structure and 3 mitoses per 10 high-power fields (40x). IHC analysis confirmed a sparsely granulated somatotrophic neuroendocrine tumor, showing diffuse synaptophysin expression, focal weak GH expression, and cytoplasmic CAM5.2 expressions, with no prolactin expression. The Ki-67 proliferation index in "hot spots" was high, reaching 11%. A focal reaction to somatostatin receptor subtypes 2A and 5 was also observed (6 points on the IRS scale). In the early postoperative period, GH levels at OGTT were 0.438 ng/ml (below 1 ng/ml), IGF-1 levels were 320.2 ng/ml (reference range: 109–479 ng/ml), and prolactin was 30.8 mIU/l (reference range: 94–557 mIU/l).

During an MRI of the brain conducted 11 months after neurosurgical treatment in April 2023, residual tumor tissue was detected in the left cavernous sinus, encircling the left internal carotid artery (ICA), measuring 18×11x21.5 mm. Additional tumor tissue was noted in the left sections of the *sella* measuring 11×10.5x8 mm, adjacent to the left contour of the infundibulum and extending toward the optic chiasm, displacing it downward. Tumor remnants were also identified in the right sections of the *sella*, measuring 10×8x6.3 mm. The patient's IGF-1 level remained elevated at 441.7 ng/ml (reference range: 109–479 ng/ml), GH was 1.08 ng/ml (reference range: 0.11–9.17 ng/ml), and prolactin was 103.2 mIU/l (reference range: 94–557 mIU/l). The ophthalmologist noted improvements in the patient's visual function. Due to persistent amenorrhea and normal blood prolactin levels, secondary hypogonadism was diagnosed, and the patient was prescribed combination therapy with dydrogesterone and estradiol.

By the summer of 2023, the patient R. has noted a deterioration in her health in the form of decreased visual acuity and periodic occurrence of diplopia. In October 2023, she experienced a sudden sharp headache on the left side, accompanied by vomiting and elevated blood pressure (145/95 mm Hg), followed by numbness on the left side of the forehead and persistent ptosis of the left eyelid. Dexamethasone (16 mg twice daily subcutaneously) was prescribed for its decongestant effect, which led to an improvement in her condition, particularly a reduction in the pressure sensation in the left eye. MRI of the brain with contrast revealed residual tumor tissue in the left cavernous sinus, encircling the left ICA and measuring 21×18x30 mm (previously 18×11x21.5 mm). This tissue was closely adjacent to the pons without signs of invasion and slightly compressing the adjacent parts of the temporal lobe, which showed signs of hemorrhagic sequelae. In the left sections of the sella, tumor tissue measured up to 20×16x13 mm (previously 11×10.5x8 mm), adjacent to the left contour of

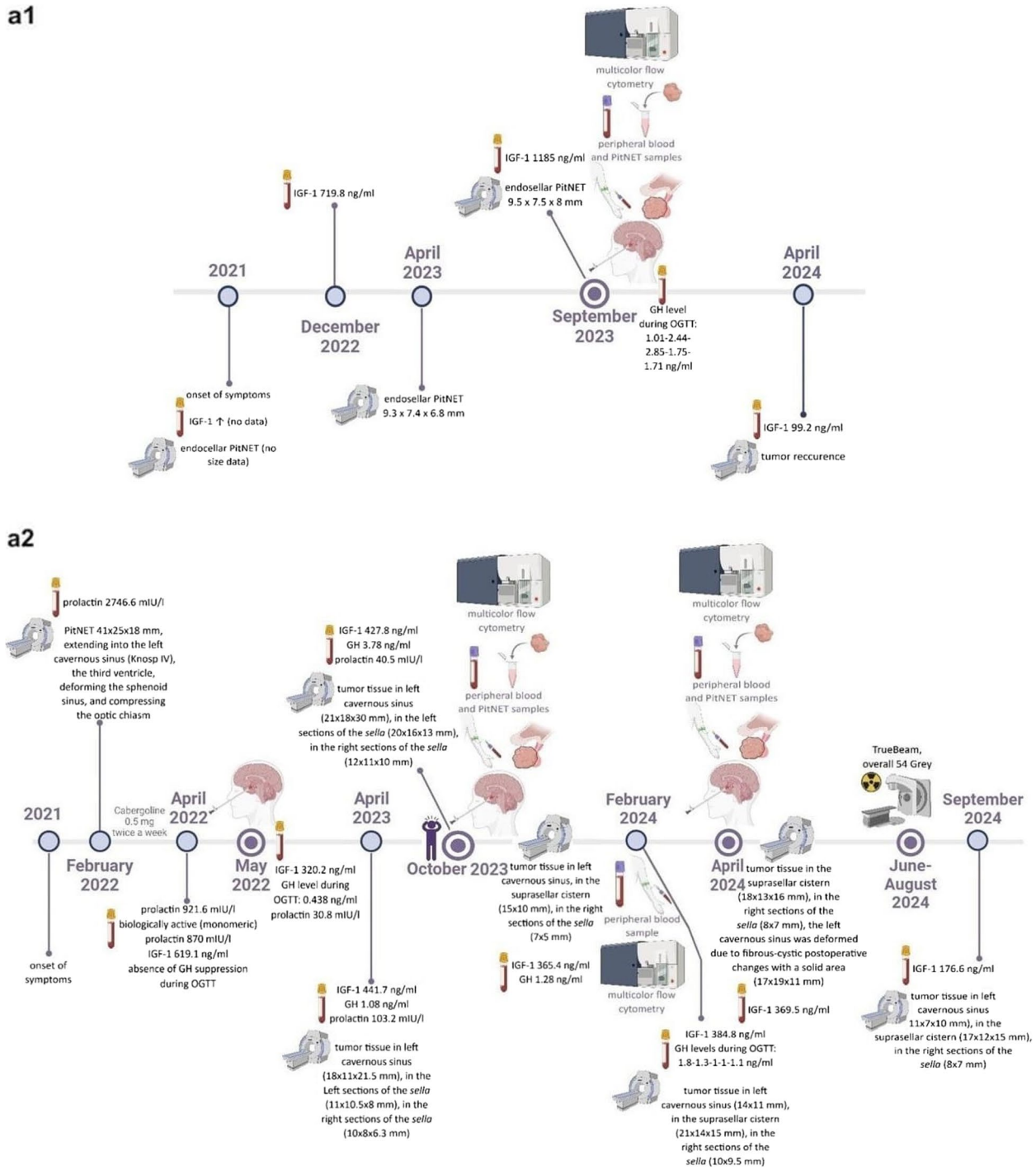

Fig. 1 Flow-chart of dynamic observation of patients. a1 refers to patient P.; a2 refers to patient R

the pituitary infundibulum and displacing and deforming the optic chiasm. In the right sections of the sella, tumor remnants measured 12×11x10 mm (previously 10×8x6.3 mm). Hormonal blood analysis showed IGF-1 levels at 427.8 ng/ml (reference range: 109–479 ng/ml), GH at 3.78 ng/ml (reference range: 0.11–9.17 ng/ml), and prolactin at 40.5 mIU/l (reference range: 94–557 mIU/l). The clinical blood analysis indicated neutrophilic leukocytosis, lymphopenia, thrombocytosis, and an elevated ESR (Table S1). Examination by an ophthalmologist

showed partial atrophy and optic neuropathy of both optic nerves, complete ptosis of the left eye, neuropathy of the left oculomotor nerve.

In October 2023, the patient underwent a repeat transnasal transsphenoidal adenomectomy. Morphological analysis confirmed a solid tumor of the adenohypophysis, consisting of eosinophilic and chromophobic cells, with one mitosis and extensive foci of fibrosis and necrobiotic changes, indicating signs of apoplexy. In the early postoperative period, IGF-1 level was 365.4 ng/ml (reference range: 109–479 ng/ml), GH was 1.28 ng/ml (reference range: 0.11–9.17 ng/ml), and the patient continued to experience decreased visual acuity, limited mobility of the left eye, and diplopia. A control MRI with contrast revealed residual tumor tissue in the suprasellar cistern, extending into the cavity of the third ventricle, compressing the chiasm, with a remnant measuring approximately 15×10 mm. Additional tissue in the right sections of the sella measured about 7×5 mm, and similar tissue continued to encircle the left ICA (Knosp IV).

During a follow-up examination in February 2024, the IGF-1 level was 384.8 ng/ml (reference range: 109–479 ng/ml). GH levels during OGTT showed no suppression: basal GH was 1.8 ng/ml; GH after 30 min was 1.3 ng/ml; after 60 min, it was 1 ng/ml; after 90 min, it was 1 ng/ml; and after 120 min, it was 1.1 ng/ml (normal suppression is less than 1 ng/ml). Prolactin was measured at 134.9 mIU/l (reference range: 94–557 mIU/l). The clinical blood test showed a slight increase in ESR and relative lymphocytosis (Table S1). MRI results indicated that residual tumor tissue measuring 14×11 mm remained in the left cavernous sinus, encircling the left ICA (Knosp IV), with additional remnants in the suprasellar cistern that compressed the chiasm and closely approached the left optic nerve, measuring 21×14x15 mm (previously 15×10x13 mm). In the right sections of the sella, the tumor measured 10×9.5 mm (previously 7×5 mm) and was deforming the medial wall of the right cavernous sinus. An ophthalmological examination confirmed anisocoria, optic neuropathy in both eyes, partial ophthalmoplegia, incomplete ptosis of the upper eyelid, and neuropathy of the left oculomotor nerve. Given the negative trend in tumor size, the neurosurgeon recommended repeated surgical intervention.

In April 2024, the patient underwent a third transnasal transsphenoidal adenomectomy. Morphological examination revealed fragments of a pituitary tumor composed of eosinophilic and chromophobic cells, characterized by a solid structure and extensive foci of hemorrhage, with adjacent areas of the adenohypophysis. The tumor was classified as fragmented. The IHC profile indicated a densely granulated somatotrophic neuroendocrine tumor of the pituitary gland, with synaptophysin and somatotropic hormone expression in single cells, and CAM5.2 staining showing fibrous bodies in small quantities. No prolactin expression was detected, and the Ki-67 labeling index was 15.0%. Moderate expression of somatostatin receptors subtype 2 was noted on the membranes of 50–60% of tumor cells (6 points according to the IRS), while moderate expression of subtype 5 was found on 70–80% of tumor cells (6 points according to the IRS). During preoperative preparation in April 2024, the ESR remained elevated (Table S1).

In the early postoperative period, an MRI of the brain with contrast showed no tumor tissue in the *sella turcica*; however, in the suprasellar cistern, heterogeneous solid tissue measuring approximately 18×13x16 mm (previously 21×14x15 mm) remained, compressing the chiasm and adjacent to the left optic nerve at the entrance to the bony canal. In the right sections of the *sella turcica* and right cavernous sinus, a heterogeneous cystic-solid tissue structure was observed, with an oval-shaped solid area exhibiting slow contrast accumulation, measuring about 8×7 mm (previously 10×9.5 mm, classified as Knosp I). The left cavernous sinus was deformed due to fibrous-cystic postoperative changes, with a solid area primarily in the posterior sinus sections, encircling the left ICA and measuring 17×19x11 mm (Knosp IV). IGF-1 level was 369.5 ng/ml. In June–August 2024 a stereotactic radiation therapy (TrueBeam, 30 fractions of 1.8 Gray over 6 weeks, overall 54 Grey) was performed. The level of IGF-1 in September 2024 was 176,6 ng/ml (102–351), MRI described a decrease in tumor size in the left cavernous sinus to 11×7x10 mm (Knosp IV), in suprasellar area to 17×12x15 mm and stabilization of tumor size in right cavernous sinus to 8×7 mm (Knosp I). The patient continues to be under dynamic observation.

Results

Any tumor, including PitNETs, is a systemic disease that reorganizes the immune system both locally and systemically [37]. The immune response to tumorigenesis is a coordinated process in all tissues—in the periphery, in secondary lymphoid organs, and in the tumor-affected organ. In this regard, we compared the subpopulations of lymphoid and myeloid cells of two patients in peripheral blood and in PitNET tissue as well as between each other using multicolor flow cytometry (protocol and methodology are in Supplementary Material 1).

Two patients' peripheral blood and PitNET samples were analyzed using four distinct multicolor cytometric antibody panels to assess the presence and distribution of various immunocompetent cell subpopulations. Panel №1 consisted of an antibody cocktail designed to

analyze major lymphocyte subpopulations, their differentiation into memory cells based on CD45RO expression and functional status by PD-1 expression. Panel №2 was designed to analyze the cytotoxic potential of CD8 + T-cells and NK-cells by examining the expression of cytolytic molecules, specifically perforin and granzyme B, as well as activation molecules CD38 and HLA-DR. Antibody panels №3 & №4 were designed to analyze myeloid cell subpopulations, including monocytes, macrophages, and myeloid-derived suppressor cells (MDSCs).

The blood and adenoma of patient P. were analyzed only once. Patient R., who experienced a recurrence, visited our center on multiple occasions. Her adenoma was analyzed two times, following surgeries in October 2023 and April 2024, and her blood was analyzed three times, prior to surgeries and between surgeries, in February 2024. Hereby, we studied two female patients, aged 63 and 20 years old, respectively. Immunophenotyping of blood and PitNET-infiltrated leukocytes of patient P. was conducted at the time of surgery due to the initial diagnosis of somatotropinoma. One year has elapsed since the surgery, and no signs of recurrence have been confirmed by the time of publication. We followed up changes in blood and PitNET leukocytes of patient R. from the date of surgery for the initial recurrence of somatotropinoma to the date of surgery for the second recurrence occurred five months later.

Peripheral blood: lymphocyte subpopulations (panel №1)

Patient P, aged 63

The clinical blood analysis (CBA) yielded unremarkable results, with the exception of a slight decrease in the absolute number of monocytes that reached 0.24*10^9 kL/L, a value that falls below the normal range of 0.3–1*10^9 kL/L (Table S1). The representative cytometric data for the analysis of the principal lymphocyte subpopulations in the blood are presented in Fig. S1.

All major lymphocyte populations (T-, B-, and NK-cells) were within the normal range, with T-lymphocytes representing the majority (83.2%)—Fig. 2, a1. The ratios between the subpopulations of NK-cells in patient P. were within the normal range. In the structure of T cells, there was an increase in the subpopulation of cytotoxic CD8 + T cells, which was accompanied by a decrease in the immunoregulatory index (IRI), defined as the ratio of CD4/CD8 T cells—Fig. 2, b1. The CD3 + CD4 + lymphocyte population was predominantly composed of CD3 + CD4 + CD25 + activated cells (46.1%), while the proportion of CD3 + CD4 + cells expressing the regulatory, inhibitory lymphocyte activation molecule PD-1 was within the normal range (2.66%,—Fig. 2, b4). The number of regulatory T cells (Tregs) was also within the normal range—Fig. 2, c1. The number of naïve CD3 + CD4 + CD45RA + cells was less than memory CD3 + CD4 + CD45RA- cells. This trend was also observed in the case of Tregs. Conversely, the majority of CD3 + CD8 + cells were naive cells (67.7%)—Fig. 2, b2-b3. Additionally, the expression of the PD-1 marker was within the normal range and amounts to 2.34% (Fig. 2, b5, Table 1).

Patient R., aged 20

At the time of the patient's R. first relapse in October 2023, patient R. took dexamethasone at a dosage of 32 mg per day. According to the CBA data, there was a notable elevation in leukocytes, reaching 14.01*10^9 kL/L. Additionally, the leukocyte profile exhibited a shift towards neutrophils (82.8%—11.61*10^9 kL/L), accompanied by a reduction in the relative number of lymphocytes (14.1%), with their absolute number remaining within the normal range. Monocyte values were approaching the lower limits of the reference range. By April 2024, all parameters exhibited positive dynamics, and a slight relative lymphocytosis was observed in February 2024 (Table S1).

FC data demonstrated a disruption in the cellular immunity balance at the initial relapse manifested by a reduction in the relative number of NK-cells and an increase in B cells up to 38.3%, and a decrease in T cells (61.3%) to a level below the normal range. By April 2024,

(See figure on next page.)

Fig. 2 Distribution of lymphocyte subpopulations in blood: comparison between healthy donors and two patients. a1 – distribution of T-cells; a2 – distribution of B-cells; a3 – distribution of NK-cells; a4 – distribution of NK-cell subpopulations; b1 – distribution of CD4 + & CD8 + subpopulations gated from CD3 + T-cells; b2 – distribution of CD45RA + naïve and CD45RA- memory CD4 + T-cells; b3—distribution of CD45RA + naïve and CD45RA- memory CD8 + T-cells; b4—distribution CD4 + T-cells with PD-1 expression; b5—distribution CD8 + T-cells with PD-1 expression; c1—distribution of Tregs; d1 – distribution of perforin + lymphocytes; d2 – distribution of Granzyme B + lymphocytes; c1—distribution of Tregs; d1 – distribution of perforin + lymphocytes; d2 – distribution of granzyme B + lymphocytes; d3—distribution of perforin + Granzyme B + NK-cells; d4—distribution of perforin + granzyme B + CD8 + T-cells; e1 – perforin-mediated cytotoxicity index of CD8 + T-cells; e2 – granzyme B-mediated cytotoxicity index of CD8 + T-cells; e3 – perforin-mediated cytotoxicity index of CD16 + NK-cells; e4 – granzyme B-mediated cytotoxicity index of CD16 + NK-cells; e5 – perforin-mediated cytotoxicity index of CD56 + NK-cells; e6 – granzyme B-mediated cytotoxicity index of CD56 + NK-cells; Data for healthy donors are represented as medians ± SE; Data for both patients are represented as values of their relative frequencies. HD refers to healthy donors, P. – patient P., R.1 – Patient R. measurement 1 in October 2023 at the first relapse; R.2 – Patient R. measurement 1 in February 2024 between relapses; R.3 – Patient R. measurement 3 in April 2024 at the second relapse; * refers to the difference from HD; ** refers to the difference between patients; *** refers to difference between the measurements of Patient R

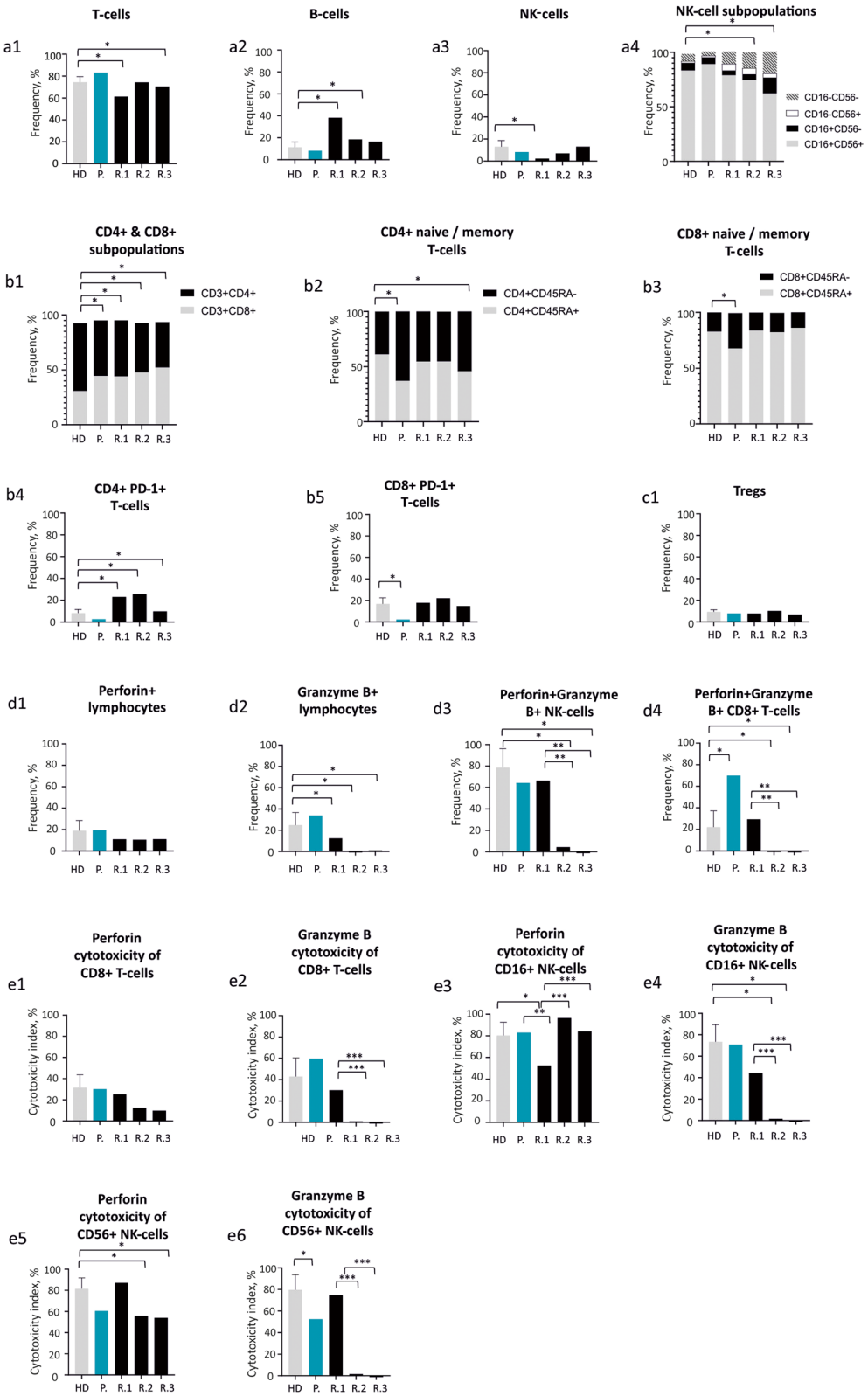

Fig. 2 (See legend on previous page.)

Table 1 Common cellular immune parameters measured with flow cytometry (panel №1) in blood and PitNET tissue from two patients (patient P—primary and patient R—recurrent disease)

	Reference Intervals, Blood, % *n* = 31, **n* = 5	Patient P., blood, %	Patient R., blood October 2023, %	Patient R., blood February 2024, %	Patient R., blood April 2024, %	Patient P., PitNET, %	Patient R., PitNET, October 2023, %	Patient R., PitNET, April 2024, %
Percentage of CD45 + leukocytes						1.75	29.9	62.8
Percentage of lymphocytes infiltrating PitNET (out of all events)						0.75	7.42	28.2
Percentage of lymphocytes infiltrating PitNET (out of all leukocytes)						30.2	23.4	50.9
CD3-CD20 + B-cells out of all lymphocytes	7.2–15.3	8.18	38.3	18.5	16.4	1.33	11.3	0.62
CD3-CD20- NK-cell out of all lymphocytes	6.9–21.5	8.3	2.33	7.12	13.1	14.2	5.57	57 >
CD3 + CD20 + CD16 + CD56 + effector NK-cells	76.7–93.7	89.2	78.9	74.2	62.4	15.6	34.3	25.3
CD3 + CD20 + CD16 + CD56- cytolytic NK-cells	1.8–8.2	6.19	4.39	5.63	14.4	15.6	4.63	2.53
CD3-CD20- CD16-CD56 + cytokine-producing NK-cells	0.7–5.3	1.5	6.04	5.61	3.63	53.1	5.56	66.6 >
CD3-CD20- CD16-CD56- immature NK-cells	0.6–12.8	3.13	10.7	14.5	19.6	15.6	50.9 >	5.5
CD3-CD16 + NK-cells out of all lymphocytes	6.6–20.5	8.03	2.03	6.73	9.94	4.42	1.6	16.6
CD3-CD56 + NK-cells out of all lymphocytes	6.2–20.1	7.33	1.94	6.44	8.84	9.29	2.54	48.6 >
CD3-CD8 + NK-cells out of all lymphocytes	1.9–10.4	2.78	0.76	2.89	2.82	1.35	0.93	3.9
CD3 + CD16 + NKT-cells out of all lymphocytes	0.4–9.5	0.75	0.15	0.47	0.53	2.21	0.67	1.58
CD3 + CD56 + NKT-cells out of all lymphocytes	2.5–9.0	5.05	2.03	5.33	1.78	51.8 >	8.22	25.2 >
CD3 + CD20- T-cells out of all lymphocytes	66.9–79.6	83.2	61.3	74.3	70.5	84.1	81.9	42.3
CD3 + CD8 + T-cells out of all T-cells	24.1–35.3	44.5	44.1	47.6	52.2	69.9 >	3.72 <	20.9
CD3 + CD4 + T-cells out of all T-cells	52.2–69.1	50.5	51	45	41.3	24.7	58.6	55.3
Tregs	7.52–11.7	7.83	7.7	10.1	6.7	0	34.8 >	19.4
Tregs naive	44.1–64.7*	26.6	45.7	59.1	45.1	NA	0.72	0.46
Tregs memory	35.1–55.7*	73.1	54	40.7	54.9	NA	99.3	97.7
PD-1 + Tregs	7.5–11.5*	8.71	13.1	11.7	6.1	NA	11.2	91 >
CD3 + CD8 + CD4 + DP T-cells out of all T-cells	0.4–2.8	4.16	1.67	2.84	1.16	1.58	36.8 >	22 >
CD3 + CD8-CD4- DN T-cells out of all T-cells	2.8–12.9	3.5	3.18	4.51	5.27	4.74	0.91	4.16
CD3 + CD4 + T-cells out of all lymphocytes	38.3–53.5	42.7	31.6	33.7	29.9	22.1	71.4	28.5
CD4 + CD25 + T-cells	9.7–18.4*	46.1	36.9	25	22.5	0	28.4	13.3
CD4 + PD-1 + T-cells	4.5–10.1*	2.66	23.1	25.7	9.84	6	6.67	78.4 >
CD4 + CD45RA + naïve CD4 + T-cells	52.5–71.6*	37	54.6	54.8	45.9	12	6.58	5.65
CD4 + CD45RA- memory CD4 + T-cells	28.3–47.5*	63	45.4	45.1	54.1	88	93.4	93.7
CD3 + CD8 + T-cells out of all lymphocytes	18.4–28.2	37.6	28.1	38.5	37.7	59.7	30.9	17.4
CD8 + PD-1 + T-cells	10.3–22.8*	2.34	17.8	22.1	14.8	4.44	2.6	62.3 >
CD8 + CD45RA + naïve CD8 + T-cells	78.2–91.6*	67.7	83.7	82.2	86.2	20.7	22.8	28.4
CD8 + CD45RA- memory CD8 + T-cells	8.3–21.7*	31.6	16.1	17.3	13.8	79.3	77	71.7
IRI (CD4/CD8) out of all lymphocytes	1.3–2.9	1.13	1.12	0.88	0.79	0.37	2.3	1.64
IRI (CD4/CD8) out of T-cells	2.9–3.8*	1.13	1.16	0.95	0.79	0.35	15.75 >	2.65

Notations: > strong overperformance; < underperformance

*refers to the parameters in control group with n=5

at the time of surgery for the second relapse, the equilibrium of T, B, and NK cell populations in the peripheral blood had been restored to normal, (Fig. 2, a1-a3, Table 1).

At the time of the initial relapse, the predominant subpopulation among NK-cells was effector CD16 + CD56 + (78.9%) NK-cells. The young regulatory CD16-CD56 + cytokine-producing NK-cells constituted 10.7%, with the immature CD16-CD56- NK-cells emerging. From October 2023 to April 2024, the following dynamics were observed: an increase in the immature (CD16-CD56-) and lytic (CD16 + CD56-) NK subpopulations, which was accompanied by a decrease in the effector (CD16 + CD56 +) and (CD16-CD56 +) cytokine-producing cells reaching 62.4% and 3.63%, respectively. As the disease progressed, a notable imbalance among NK subpopulations was observed (Fig. 2, a4, Table 1).

Follow-up observation of T-cell immunity in patient R. revealed a slight increase in the relative number of T lymphocytes based on the increase in CD3 + CD8 + cytotoxic T cells, while the CD3 + CD4 + T cells demonstrated a more stable level (Fig. 2, b1). The IRI showed a notable decline from 1.12 to 0.79. Additionally, a slight fluctuation in the number of regulatory T cells (Tregs) was observed, within a range from 7.7% to 10.1% to 6.7% (Fig. 2, c1, Table 1). Frequency of activated CD3 + CD4 + CD25 + T-lymphocytes reduced from 36.9% to 22.5%. As the disease progressed, there was a notable shift in the balance of naive and memory T cells, with an increase in the proportion of CD3 + CD4 + CD45RA- memory cells (from 45.4% to 54.1%)—Fig. 2, b2-b3. Concomitantly, the expression of PD-1 also decreased, from 23.1–25.7% to 9.8%, in both CD3 + CD4 + cells and Tregs—Fig. 2, b4. A steady prevalence of naive cells (83.7–86.2%) was observed among CD3 + CD8 + T-cells. PD-1 expression exhibited slight fluctuations – (Fig. 2, b5, Table 1).

It is therefore worth highlighting the following characteristics of lymphocyte immunophenotype of the two patients: the number of T lymphocytes was higher in patient P. than in patient R.—Fig. 2, a1. The IRI was reduced in both patients; in patient R. it demonstrated a tendency to decrease as the disease progressed. It should be noted that IRI decreases with age, in endocrine diseases, solid tumors [38]. The number of CD3 + CD4 + cells, including activated (CD3 + CD4 + CD25 +) cells, was higher in patient P than in patient R. Furthermore, there was a tendency for these subpopulations to decrease with disease progression in patient R. The proportion of CD3 + CD4 + PD1 + also decreased in patient R over time, yet remained higher than in patient P—Fig. 2, b4. The number of Tregs was comparable in both patients—Fig. 2, c1. Memory CD3 + CD45RA- CD4 + T-cells were more prevalent than naive cells in patient P, whereas in patient R there was a tendency for their increase with time—Fig. 2, b2. The number of CD3 + CD8 + T-cells (out of all lymphocytes) in patient R. at the time of surgery for the first relapse and in association with immunosuppressive therapy was diminished in comparison to patient P. As the disease progressed, this parameter reached values comparable to those of patient P—Fig. 2, b1. In both patients, naive CD3 + CD45RA + CD8 + T-cells prevailed over memory cells, with their higher frequency in patient R.—Fig. 2, b3. This could be attributed to the younger age of the relapsed patient, as the number of naive T cells is known to decline with age [39]. Furthermore, PD-1 expression by CD8 + T-cells was enhanced in patient R. compared to patient P.—Fig. 2, b5.

Slight variations in the number of T lymphocytes observed in patient R over time were accompanied by the sustained reduction of B-cells and the increase of NK-cells. Yet patient R. restored her TBNK balance to the normal ranges, her B-cell numbers remained higher than that of Patient P. Also during the course of patient P's disease, there was a decrease in the relative number of effector CD16 + CD56 + and a growth of the proportion of immature CD16-CD56- cells among NK-cells. The balance between these subpopulations in patient P was within the normal range. The observed increase in the total NK cell population in this case might therefore serve to compensate for the lack of effector NK cells. The case of patient R. served to illustrate that the balance of lymphocyte subpopulations underwent changes as the disease progressed. The activation of T lymphocytes decreased, while the number of naive T lymphocytes remained high.

PitNETs: lymphocyte subpopulations (Panel №1)

Cytometric dot plots and gating strategy regarding tumor-infiltrating lymphocyte (TIL) subpopulations are presented in Fig. S2.

Patient P, aged 63 years, was diagnosed with a densely granulated somatotroph neuroendocrine tumor of the pituitary gland, for which she underwent her surgical intervention. The patient's PitNET was infiltrated with a low percentage of TILs reaching 0.75% out of all cells and 30.2% out of all leukocytes (Table 1). TILs were predominantly composed of CD3 + CD20- T cells (84.1%), with NK and B cells amounting to 14.2% and 1.33%, respectively (Fig. 3, a1-a3). The relative number of cytotoxic CD3 + CD8 + lymphocytes (69.9%) were approximately 3 times higher than CD3 + CD4 + T helpers (22.1%), and thus IRI equaled 0.37. Double positive (DP) CD4 + CD8 + T-cells constituted 1.58%. Memory

cells constituted about 80% in both CD3 + CD4 + and CD3 + CD8 + T-cell subpopulations. Additionally, low PD-1 expression was observed in both subpopulations, and no activated CD3 + CD4 + or Tregs were present—Fig. 3, c1. CD56 + NKT lymphocytes (51.8%) were particularly abundant. Cytokine-producing NK-cells constituted about 50% of the total NK-cells, while other NK subpopulations, including effector, lytic, and immature cells were found at a similar frequency (approximately 15.6% each) (Table 1).

Patient R, aged 20. The patient R. was twice admitted with a recurrence of a sparsely granulated somatotroph neuroendocrine tumor of the pituitary gland. At the time of the TIME analysis following the second recurrence, three traumatic surgical procedures involving brain tissue and violating the integrity of the cavernous sinus had been performed. Dexamethasone administration was prescribed including the day of surgery for the first recurrence. Unfortunately no data were available on the composition of TILs for patient R at the initial diagnosis. Nevertheless, an evaluation of the process dynamics could be conducted based on the data obtained from two relapses.

At the time of the surgery for the first relapse, the operative material demonstrated that TILs constituted 7.42% out of all PitNET cells and 23.4% of all leukocytes. Following the second relapse of the disease and surgical intervention, the number of TILs increased to 28.2% out of all cells, constituting 50.9% out of all leukocytes. Among TILs in the first relapse, T cells were predominant lymphocytes (81.9%), of which there were 71.4% CD3 + CD4 + cells and 30.9% CD3 + CD8 + cells (IRI = 2.3). Within the CD3 + CD20- T-cells we observed 58.6% CD3 + CD4 + CD8- and 3.72% CD3 + CD8 + CD4-, and a high level of CD3 + CD4 + CD8 + DP T lymphocytes reaching 36.8%—Fig. 3, b1. IRI value was 15.75 (Table 1). Among CD3 + CD4 + cells, including CD8-positive cells, CD25 expressed in 28.4% of cells, while PD-1 expression was observed in 6.67% of cells—Fig. 3, b4. The majority of CD4 + T-cells (93.4%) exhibited a memory CD3 + CD4 + CD45RA- phenotype—Fig. 3, b2. There were 34.8% Tregs isolated from 71.4% of CD3 + CD8-CD4 + T-cells—Fig. 2, c1. Among CD3 + CD8 + cells, including CD4-positive cells, 2.26% cells expressed PD-1—Fig. 3, b5. Memory CD3 + CD8 + CD45RA- cells (77.0%) prevailed over naive cells (Table 1)—Fig. 3, b3.

The analysis of TILs in the pituitary tissue after intervention for the second recurrence demonstrated a shift in the lymphocyte TBNK balance towards NK-cells—Fig. 3, a1- a3. The number of T lymphocytes decreased to 42%. Additionally, alterations were observed among T-cells. The number of CD3 + CD4 + CD8 + DP T-cells decreased to 22%, while CD3 + CD4 + CD8- lymphocytes and CD3 + CD8 + CD4- lymphocytes reached 55.3% and 20.9%, respectively—Fig. 3, b1. Consequently, IRI calculated from T-cell subpopulations without considering CD4 + CD8 + co-expression equaled 2.65. CD25 expression decreased to 13.3% among CD3 + CD4 + cells including CD8-positive cells. In contrast, PD-1 expression significantly increased to 78.4% among CD3 + CD4 + cells and to 62.3% among CD3 + CD8 + T-cells (Fig. 3, b4-5). Tregs number drastically reduced to 19.4%. The ratio between naive and memory cells in the CD3 + CD4 + and CD3 + CD8 + populations, as well as among Tregs remained unaltered, taking into account double positive events. As the disease progressed, the number of CD56 + NKT cells increased from 8.22% to 25.2%. Furthermore, not only did NK-cells increase in the number from 5.57% to 57%—Fig. 3, a3, but alterations in their structure accompanied the second relapse. The proportion of cytokine-producing CD16-CD56 + NK-cells grew from 5.56% to 66.6% along with a reduction CD16 + CD56 + effector NK-cell (from 34.3% to 25.3%) and immature CD16-CD56- NK-cells (from 50.9% to 5.5%)—Fig. 3, a4. Thus, the increase in NK-cells was primarily attributable to CD3-CD56 + subpopulation, which constituted 48.6% of all lymphocytes, while CD3-CD16 + cells contributed only 16.6% (Table 1). The alterations in lymphocyte balance impacted B-cells also, with a notable decline in their frequency from 11.3% to 0.6%—Fig. 3, b2.

(See figure on next page.)

Fig. 3 Distribution of lymphocyte subpopulations in the patients' PitNets: comparison between two patients. a1 – distribution of T-cells; a2 – distribution of B-cells; a3 – distribution of NK-cells; a4 – distribution of NK-cell subpopulations; b1 – distribution of CD4 + & CD8 + subpopulations gated from CD3 + T-cells;; b2 – distribution of CD45RA + naïve and CD45RA- memory CD4 + T-cells; b3—distribution of CD45RA + naïve and CD45RA- memory CD8 + T-cells; b4—distribution CD4 + T-cells with PD-1 expression; b5—distribution CD8 + T-cells with PD-1 expression; c1—distribution of Tregs; d1 – distribution of perforin + lymphocytes; d2 – distribution of Granzyme B + lymphocytes; d3—distribution of perforin + granzyme B + NK-cells; d4—distribution of perforin + granzyme B + CD8 + T-cells; e1 – perforin-mediated cytotoxicity index of CD8 + T-cells; e2 – granzyme B-mediated cytotoxicity index of CD8 + T-cells; e3 – perforin-mediated cytotoxicity index of CD16 + NK-cells; e4 – granzyme B-mediated cytotoxicity index of CD16 + NK-cells; e5 – perforin-mediated cytotoxicity index of CD56 + NK-cells; e6 – granzyme B-mediated cytotoxicity index of CD56 + NK-cells; f1 – frequency of macrophages among all cell types in PitNETs; f2 – distribution of macrophage M1 and M2 subpopulations; Data for both patients are represented as values of their relative frequencies. HD refers to healthy donors, P. – patient P., R.1 – Patient R. in October 2023 at the first relapse; R.2 – Patient R. in April 2024 at the second relapse; * refers to the difference between patients; ** refers to the difference between two relapses of Patient R

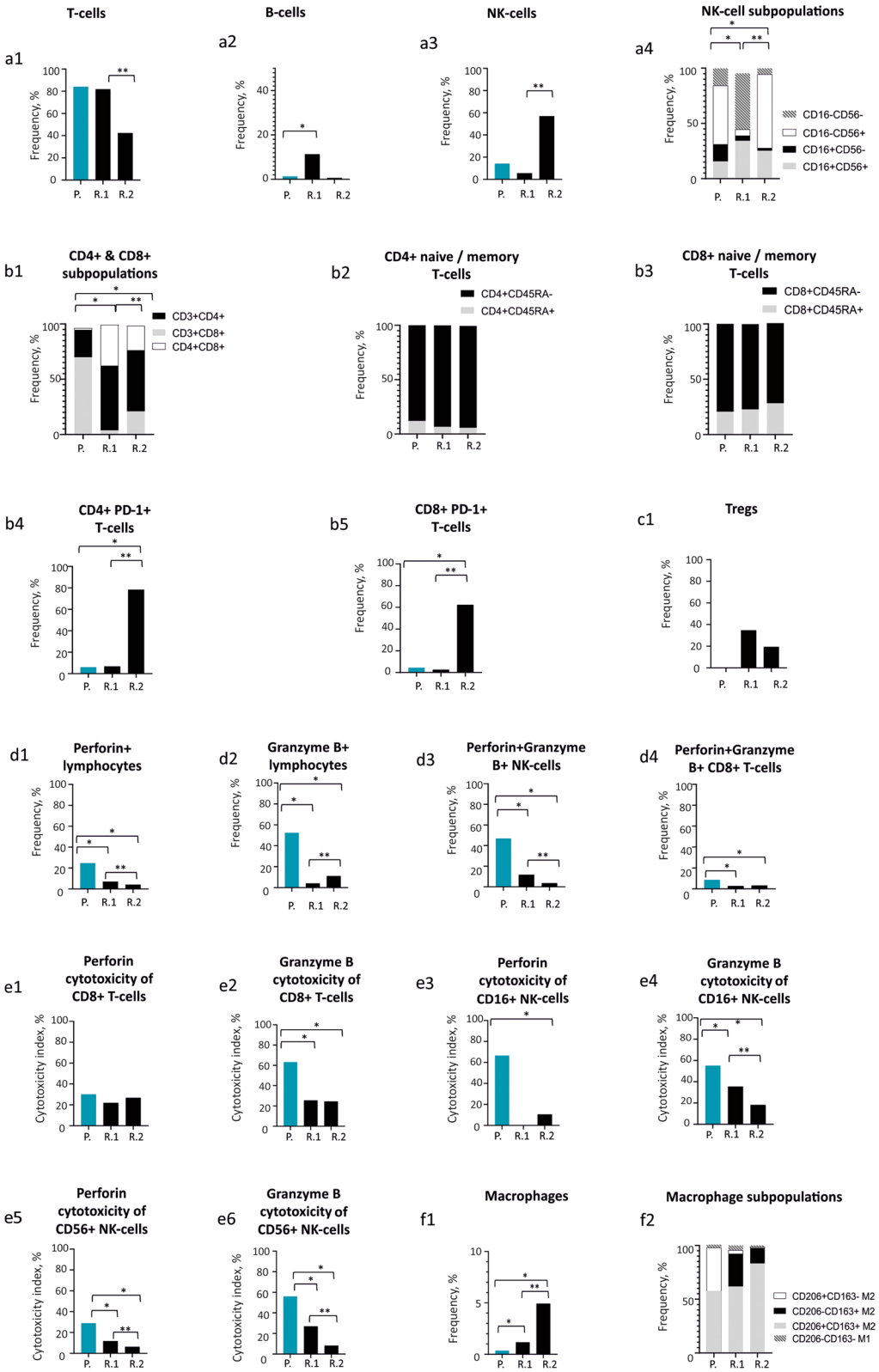

Fig. 3 (See legend on previous page.)

The summary of the data on TILs in both patients revealed several noteworthy trends. Both patients exhibited a high number of memory T cells in the pituitary tissue, across both the CD3+CD4+and CD3+CD8+populations Fig. 3, b1-2. Furthermore, the ratio of memory cells to naive lymphocytes remained unaltered throughout the course of the disease. The number of T lymphocytes in patient P. and in patient R. at first relapse in pituitary tissue was comparable. Both exhibited low expression of PD-1 on CD3+CD4+and CD3+CD8+T cells.

It is evident that patient R., who experienced tumor progression in the pituitary tissue and underwent traumatic surgical procedures, exhibited a markedly different TIME than patient P. The structure of T- and NK-cells in these two patients differed dramatically. Therefore, although the number of T lymphocytes declined in patient R. over time, the subpopulation composition differed from that of patient P. by exhibiting a predominance of CD3+CD4+lymphocytes over CD3+CD8+, and a substantial presence of CD3+CD4+CD8+DP cells (Fig. 4). The appearance of DP T cells, which frequently arise from CD4+T-cells and subsequently acquire the phenotype and properties of CD8+T-cells under constant stimulation of their TCRs by tumor antigen, has been observed among TILs of different tumor types [40]. Also the second recurrence of the tumor process in pituitary tissue in patient R. was accompanied by a significant increase in PD-1 expression on CD3+CD4+and CD3+CD8+T cells (Fig. 3, b4-b5) and Tregs. Chronic tumor-specific TCR stimulation has been demonstrated to induce long-term persistent PD-1 expression, which ultimately results in the functional depletion of T cells and the attenuation of their anti-tumor activity [39].

Peripheral blood: cytotoxic potential of CD8+T-cells and NK-cells (panel №2)

The granule-mediated cytotoxicity of effector cells represents one of the key mechanisms underlying their cytotoxic action against tumor growth and the induction of target cell death. Granzyme B is the primary mediator of the cytolytic activity of effector cells, while perforin is responsible for the delivery of this protein to the target cell. Fig. S3 illustrates the gating strategy of FC data at evaluating the granule-mediated cytotoxic potential. The proportion of CD3+and CD3- cells expressing perforin or granzyme B was determined. Additionally, the proportion of cytotoxic CD3+CD8+T cells and NK cells expressing both types of granules, perforin and granzyme B, independently or simultaneously was estimated. Eventually, the cytotoxic index (CI) of CD3+CD8+T cells and CD16+and CD56 NK cells was calculated based on the expression of perforin and granzyme. The results of the analysis of cytotoxic potential of the main lymphocyte populations are presented in Table 2, Figs. 2 and 3.

Furthermore, we estimated CD8 and CD38 expression on NK cells. NK cells that express CD8 (CD3-CD8+NK) typically carry CD8α homodimer, which protects them from apoptosis following target cell encounter and its lysis. In other words, CD3-CD8+NK cells are protected from activation-induced apoptosis and have the capacity for multiple lysis of target cells [42]. The signal from CD38 in activated NK cells elicits a cytotoxic response, granzyme release, and cytokine secretion. The association of CD38 and CD16 is crucial for NK cells to develop an effector cytotoxic phenotype [43]. Human leukocyte antigen-DR (HLA-DR) or major histocompatibility complex type II molecule (MHC class II) is frequently regarded in clinical settings as

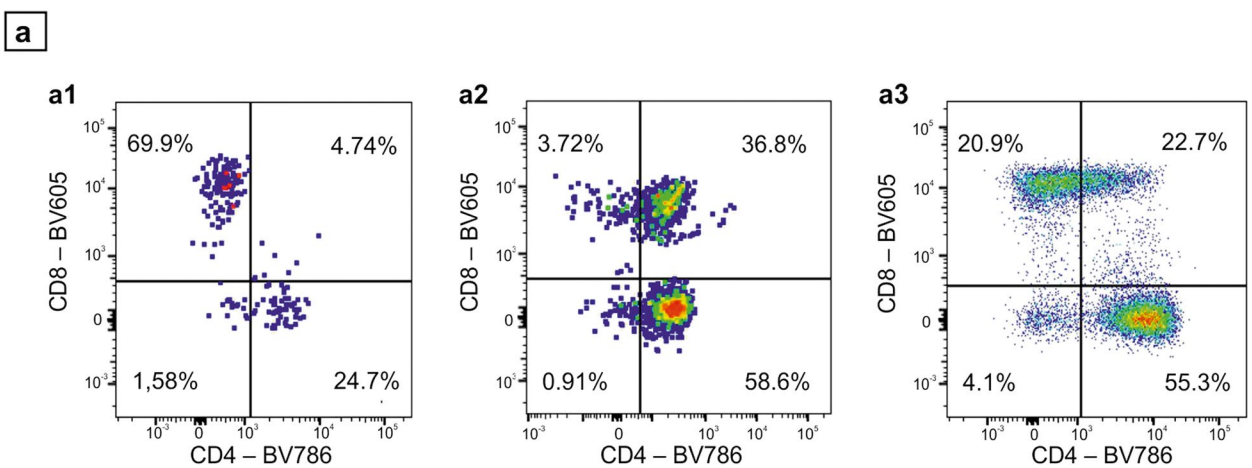

Fig. 4 The comparative distribution of CD3+T-cells infiltrating adenomas from two patients on CD4-BV786/CD8-BV605 dot plots. a1—Patient P; a2 Patient R, first relapse in October 2023; a3—Patient R, second relapse in April 2024

Table 2 The parameters of granule-mediated cytotoxic potential determined via flow cytometry analysis (Panel №2) in the blood and PitNETs tissue of two patients (patient P with primary disease, and patient R, who experienced a relapse)

	Reference Intervals, Blood, %, $n = 23$, *$n = 5$	Patient P., blood, %	Patient R., blood October 2023, %	Patient R., blood February 2024, %	Patient R., blood April 2024, %	Patient P., PitNET, %	Patient R., PitNET, October 2023, %	Patient R., PitNET, April 2024, %
CD3-Perforin + cells out of all lymphocytes	5.4–16.1	8.74	2.34	7	9.95	9.06	0.67 <	2.81
CD3-GranzymeB + cells out of all lymphocytes	4.7–15.3	7.06	1.64 <	0.12 <	0.19 <	6.3	0.39 <	4.57
CD3 + Perforin + cells out of all lymphocytes	4.3–13.3	10.8	8.69	3.57	1.12 <	15.7	6.33	1.42
CD3 + GranzymeB + cells out of all lymphocytes	7.4–19.9	26.8	10.5	0.38 <	0.86 <	46.1 >	3.65	6.43
Perforin + cells out of all lymphocytes (Sum)	12.7–26.5	19.54	11.03	10.57	11.07	24.76	7.0	4.22
GranzymeB + cells out of all lymphocytes (Sum)	14.4–32.9	33.9	12.14	0.5 <	1.05 <	52.4	4.04	11,0
GranzymeB + Perforin + cells out of CD3-NK-cells	72.1–91.0	64.3	66.3	4.39 <	0.1 <	46.9	11.8 <	3.61 <
CD3 + CD8 + T-cells out of all lymphocytes	21.7–30.5	37.1 >	27.3	36.2 >	38.1 >	55.6	30.7	22.9
GranzymeB + Perforin + cells out of CD3 + CD8 + T-cells	6.5–30.3	69.9 >	29.4	0.44 <	0.09 <	8.7 <	2.87 <	3.28
CD8 + Perforin + cytotoxicity index, %	22.5–48.9	30.2	25.2	12.4 <	9.7 <	30.2	21.9	26.8
CD8 + GranzymeB + cytotoxicity index, %	30.4–58.6	59.7	30.1	0.9	0.3. <	63.3	25.5	24.5
CD16 + Perforin + cytotoxicity index, %	64.8–97.5	83.1	52.6	96.4	84.2	66.6	NA	10.5
CD16 + GranzymeB + cytotoxicity index, %	61.3–88.7	70.9	44.3 <	1.6 <	0.2 <	55.2	35.4	18.2
CD56 + Perforin + cytotoxicity index, %	64.3–94.7	60.6	87.1	55.7	54	29	11.8	6.3
CD56 + GranzymeB + cytotoxicity index, %	61.3–93.1	52.5	74.8	1.5 <	0.1 <	56.1	27	8.2
CD3 + CD38 + from CD45 + lymphocytes	2.1–7.1*	3.68	2.51	1.52	6.04	54.5 >	6.92	36.2 >
CD3 + CD8 + CD38 + from CD3 + CD8 + T-cells	1.3–4.9*	1.88	4.15	2.3	4.15	74.8 >	13.2	75.8 >
CD3 + HLA-DR + from CD45 + lymphocytes	0.6–2.0*	8.46 >	1.43	1.69	1.68	9.09	30.2	2.35
CD3 + CD8 + HLA-DR + from CD3 + CD8 + T-cells	0.3–2.7*	12.3 >	3.37	1.05	2.6	5.07	5.54	6.11
CD8 + CD38 + from NK-cells	3.8–36.4*	18.5	7.64	6.96	17.2	8.82	NA	10.7
CD8 + CD38-from NK-cells	5.0–20.0*	4.35	23.1 >	28.4 >	18.2	5.88	NA	0.39

Notations: > strong overperformance; < underperformance

a marker of late activation, a marker of immune reactivity. The expression of this marker can be utilized to assess the strength and magnitude of the immune response.

Patient P, a 63-year-old female

The number of perforin and granzyme B containing lymphocytes was within the normal range, amounting to 19.54% (sum of CD3 + Perforin + and CD3-Perforin +) and 33.9% (sum of CD3 + Granzyme B + and CD3-Granzyme B +), respectively – Fig. 2, d1-d2. The proportion of NK cells and CD3 + CD8 + cytotoxic cells containing perforin and granzyme B granules simultaneously was approximately equal, amounting to 64.3% and 69.9%, respectively, though exceeding the normal values for CD8 + T cells (Fig. 2, d3-d4, Table 2).

However, we observed that the density of perforin and granzyme B expression in the CD3 + CD8 + T-cell subpopulation was relatively low (Fig. 5, a1). The CI of CD8 + and CD16 + subpopulations by perforin and granzyme B was within the normal range Fig. 2, e1-e4, with a slight reduction observed for CD56 + NK cells Fig. 2, e5-e6. However, this remains within the normal limits. In general, the CD16 + subpopulation exhibits a higher degree of granule-mediated cytotoxicity.

The frequency of CD8 + NK cells exhibiting co-expression of CD8 and CD38 reached 18.5%, representing a significant subset of the total CD8 + NK-lymphocyte population (22.85%). HLA-DR was expressed by 12.3% of cells within CD3 + CD8 + T-lymphocytes.

Patient R, aged 20, female

Dynamic observation over 6 months revealed that the total number of perforin-containing lymphocytes remained unaltered, comprising approximately 11% of all lymphocytes – Fig. 2, d1. However, there was a notable shift in the balance towards CD3 + Perforin + -lymphocytes. The number of cells containing granzyme B underwent a notable decline over the course of the disease, from 12.14% to 1.05%—Fig. 2, d2, Table 2. This alteration affected both CD3- and CD3 + populations of lymphocytes. It is noteworthy that at the time of the first relapse, the total number of perforin- and granzyme-containing lymphocytes was comparable (11.05% vs. 12.14%). However, as the disease progresses, this ratio shifted towards perforin-containing cells. This was corroborated by the assessment of the number of NK cells (all NK except for the CD3-CD16-CD56- population) and CD3 + CD8 + cytotoxic lymphocytes containing simultaneously both types of granules with granzyme B and perforin—Fig. 2, d3-d4. At the time of the first relapse, the number of Granzyme B + Perforin + NK cells was 66.3% of all NK cells. However, this dropped significantly to 4.39% as the disease progressed, reaching a value of less

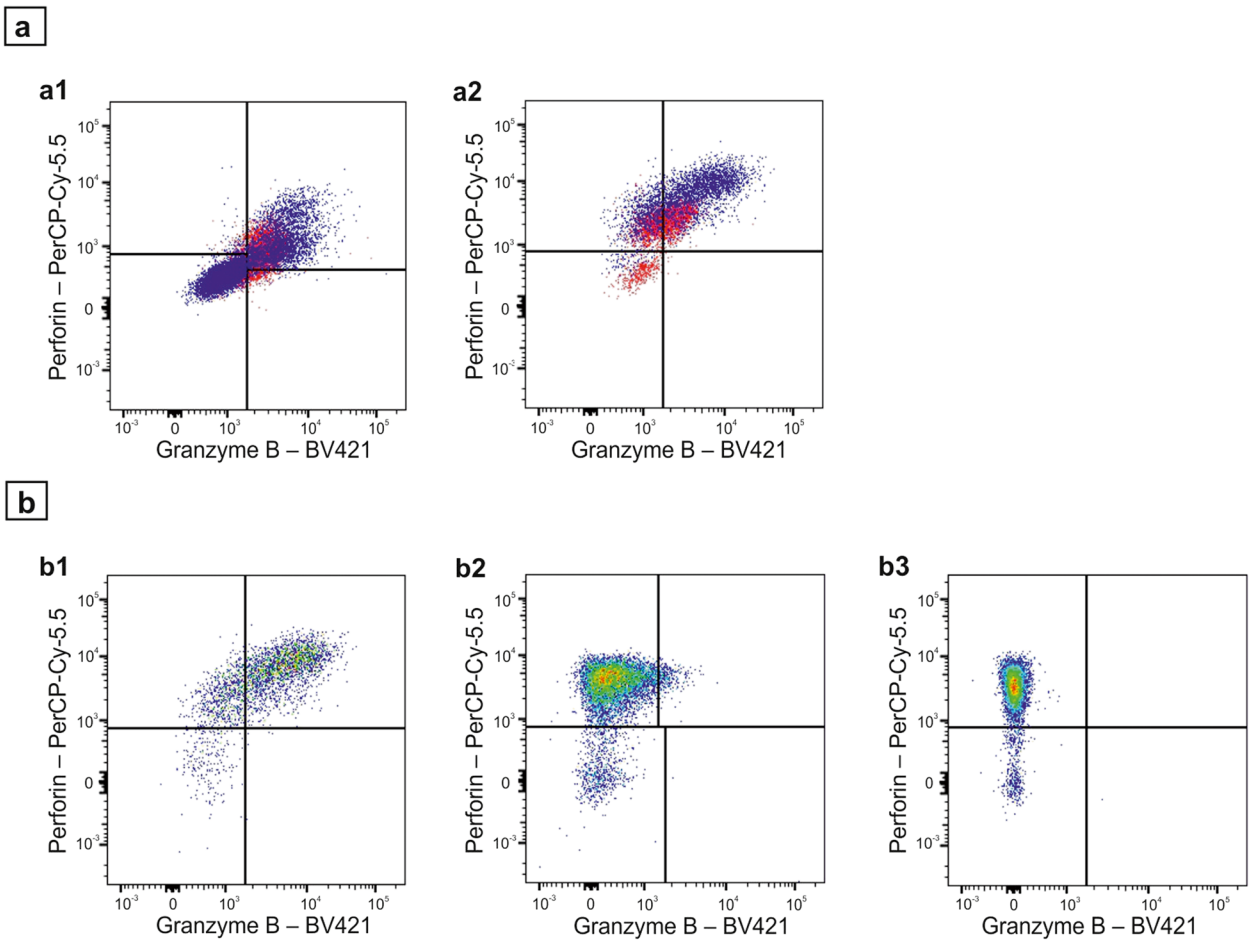

Fig. 5 The comparative dot plots observed at analyzing the cytotoxic potential of lymphocytes. **a** Distribution of CD8 + T cells (a1) and NK cells (a2) from the blood of patient P. (red) and patient R. (blue) on Granzyme B-BV421/Perforin-PerCP-Cy5.5 dot plot; **b** Distribution of NK cells from the blood of patient R on Granzyme B-BV421/Perforin-PerCP-Cy5.5 dot plot over time: b1, October 2023; b2, February 2024; b3, April 2024

than 1% at the time of the second relapse. Similarly, the percentage of CD3+CD8+lymphocytes caring both granzyme B and perforin granules at the time of the first relapse was 29.4%, while at the time of the second relapse this value was also less than 1% (Table 2). At the time of the first relapse, we observed two subpopulations of CD3+CD8 T cells expressing perforin and granzyme B distinguished by perforin expression density. However, the cells with high perforin expression level were not identified in the subsequent analysis in February and April 2024 (Fig. 5, a1).

The CI of CD8+, CD16+, and CD56+cells by granzyme B exhibited a marked decline as the disease progressed Fig. 2, e2, e4, e6. It would appear that an anergy of potential effector cells developed in conjunction with the tumor progression. The CI of CD8+and CD56+lymphocytes by perforin showed a decline, though not to such a critical level (Fig. 2, e1, e5, Table 2). In contrast, the situation is different for CD16+lymphocytes. The CI of CD16+lymphocytes containing perforin granules increases with disease progression (from 52.6% to 84.2% at the time of the second relapse—Fig. 2, e3). Observing that the number of effector CD16+CD56+NK-cells declined over time, whereas the number of lytic CD16+CD56- NK-cells increased (Table 1) we suggest that these dynamical changes in cytotoxicity of subpopulations of NK-cells might be attributable to compensatory reactions in NK-cell homeostasis.

Evaluating CD8 and CD38 expression on NK lymphocytes revealed that the number of CD8-positive cells (calculated as the sum of CD8+CD38+and CD8+CD38- cells among NK cells) remained constant (ranging from 30.7% to 35.36% to 35.4%). However, the proportion of cells expressing CD38 increased as the disease progressed, from 7.64% to 17.2%. The expression of HLA-DR remains relatively unchanged, exhibiting minimal fluctuations and maintaining a low level in both total CD3 population and the CD3+CD8+subpopulation.

A comparison of the CIs between the patients revealed the following: patient P. exhibited a higher number of granule-containing lymphocytes Fig. 2, e1-e6. Additionally, patient P. exhibited elevated CD8+granzyme B cytotoxicity, while perforin cytotoxicity remained comparable (30.2% in patient P, 26.1% in patient R, Fig. 2, e1-e2). When considering CD8 T cells that simultaneously expressed perforin and granzyme B, their number was approximately 2.3 times higher in patient P. compared to patient R. at the initial measurement Fig. 2, d4. Furthermore, the frequency of these cells in patient R. decreased from 29.4% to 0.09% (Table 2). The cytotoxicity of CD16+cells (based on CI) by perforin in patient R. was low at the time of the first relapse. However, as the disease progressed, it reached values comparable to those observed in patient P., though accompanied by the reverse dynamics of cytotoxic potential of the same population by granzyme B—Fig. 2, e3-e4. The CI for granzyme and perforin for CD56+cells in patient P. was lower than that observed in patient R. at the time of the first relapse. As the disease progressed in patient R., the CI for perforin decreased to 55.7–55%, while the CI for granzyme dropped to the value less than 1%—Fig. 2, e5-e6. The proportion of NK cells expressing both perforin and granzyme B in the blood of patient P. and patient R. at the first relapse was comparable, reaching 64.3% and 66.3%, respectively. However, within six months of the disease progression in patient R., this number decreased significantly, dropping from 66.3% to 0.1% (Fig. 2, d3, Table 2). NK cells of both patient P. and patient R. at the first relapse were characterized by the predominance of effector -CD16+CD56+NK-cells, which may explain why the number of GranzymeB+Perforin+CD3-NK in these patients was comparable (64.3% and 66.3%). However, the density of perforin and granzyme B expression was higher in patient R. at the first relapse (Fig. 5, a2). Nevertheless, within six months, the level of these cells dropped to the critical 4.39% and 0.1% (Table 2, Figs. 2, d3 and 5, b1-b3). In conclusion, there is a notable reduction in the expression of granzyme-containing lymphocytes among both CD8+T cells and NK cells.

The number of HLA-DR+lymphocytes was higher in both total CD3+T-cells and cytotoxic CD3+CD8+T-cells in patient P. Despite the lower number of CD8+expressing cells among all NK in patient P. compared to patient R., the proportion of cells expressing CD38 was significantly higher. It can be postulated that there was an increase in the number of prolonged-acting NK cells in patient P., although the level of cytotoxicity may have decreased.

PitNETs: cytotoxic potential of CD8+T-cells and NK-cells (panel №2)

The cytometric analysis of the cytotoxic potential of CD8+T cells and NK cells infiltrating the PitNETs is presented in Fig. S4.

Patient P, aged 63 years

In Patient P's adenoma, a high frequency of perforin and granzyme B-containing cells was identified within CD3+T-cells, in comparison to CD3- lymphocytes. Furthermore, almost half of CD3- NK cells were found to produce both perforin and granzyme B simultaneously (46.9%)—Fig. 3, d3. In CD8+and CD56+lymphocyte subpopulations, the calculated CI for granzyme B was approximately twice that of perforin-containing cells—Fig. 3, e1-e2, e5-e6. In case of CD16+lymphocytes, the

aforementioned indices were almost equal, with perforin-containing cells accounting for 66.6% and granzyme B-containing cells for 55.2%—Fig. 3, e3-e4. It's noteworthy, 54.5% CD3 + cells and more than 70% CD3 + CD8 + T lymphocytes expressed CD38, with a mere 9.09% and 5.07% of these cells exhibiting HLA-DR expression, respectively. Double-positive CD8 + CD38 + NK cells accounted for 8.8% of all NK lymphocytes (Table 2).

Patient R, aged 20 years

We observed the following dynamics of the number of granule-containing TILs during the disease progression: the level of perforin-containing lymphocytes decreased, while the number of cells containing granules with granzyme B increased. The number of granule-containing cells in CD3- NK cells increased with disease progression (Table 2). Concurrently, the number of cells containing granules of both perforin and granzyme B in CD3- NK cells decreased (from 11.8% to 3.61%, Fig. 3, d3), while there were minimal alterations (2.87% at the first relapse, 3.28% at the second relapse) in CD3 + CD8 + cytotoxic lymphocytes—Fig. 3, d4. The level of perforin- and granzyme B-mediated CD8 + CI remained stable (Fig. 3, e1-e2), while granzyme B-mediated CD16 + lymphocyte CI declined (data on perforin-mediated CD16 + cytotoxicity could not be obtained at the first relapse due to low number of CD16 + events)—Fig. 3, e3-e4. A similar trend was observed for CD56 + lymphocytes (both CI decreased as the disease developed, Fig. 3, e5-e6). The data on cytotoxic potential were in a good agreement with the dynamics of changes in the number of granule-containing effector cells and with changes in the structure of NK cells (by the second relapse cytokine-producing CD16-CD56 + NK cells became the prevailed subpopulation) (Tables 1 & 2). The number of CD38 + T-lymphocytes at the time of the second relapse sharply increased, reaching almost fivefold the initial value, both among CD3 + and CD3 + CD8 + T-cells. The number of T-cells expressing HLA-DR heavily decreased at the time of the second relapse; however, CD3 + CD8 + T-cells expressed HLA-DR in a sustained manner. We observed a high percentage of CD8 + CD38 + NK cells at the time of the second relapse, amounting to 10.7%. We couldn't analyze the dynamics of these cells as there appeared insufficient number of events in the gate of NK cells of the adenoma sample at the first relapse to perform statistically significant assessment (Table 2).

Comparing the cytotoxic potential of effector lymphocytes between two patients we revealed that the number of effector cells producing perforin and granzyme B, including those that produced both granule types simultaneously was markedly reduced in patient R. exhibiting a more aggressive disease course—Fig. 3, d1-d4, e1-e6. At the same time, at the second relapse, the number of NK cells in this patient constituted over 50% of all lymphocytes, with the majority exhibiting a CD3-CD56 + phenotype (Fig. 3, a4, Table 1). However, less than 6% of these cells were able to fulfill their cytotoxic potential through perforin production (Fig. 3, e5, Table 2). The similar scenario was observed for CD16 + population of patient R.—Fig. 3, e3. Whereas, perforin-mediated cytotoxicity can be achieved by 66.6% of CD16 + and 29% of CD56 + TILs in patient P.—Fig. 3, e3, e5. CD8 + cells in two patients displayed comparable values for perforin content—Fig. 3, e1. Additionally, in comparison to patient P., TIME of patient R. exhibited a diminished infiltration of granzyme B-mediated CD16 + and CD56 + effector cells both at the first relapse and by the second relapse, when CI declined up to 18% and 8%, respectively Fig. 3, e4, e6. The number of T lymphocytes expressing CD38 was also markedly lower in patient R with a more aggressive course. However, by the time of the second relapse, these indices become comparable between both patients. HLA-DR expression was comparable in both patients.

Peripheral blood: myeloid cells and myeloid suppressors (panel №3)

In addition to the analysis of lymphoid cells, we estimated the number and characteristics of some myeloid cell populations. The antibodies used in Panel №3 permitted the analysis of monocytes (CD45 + CD14 +), neutrophils (CD45 + CD16 +) and myeloid-derived suppressor cells (MDSCs). The strategy undertaken at the cytometric analysis of myeloid cells in blood are presented in Fig. S5.

The neutrophil count of patient R. exhibited fluctuations throughout the course of the disease. At the first relapse, the value was 53.4%. By February 2024, it had decreased sharply, reaching 19.3%. However, by April, the neutrophil level had already returned to its previously observed value of 50.2%. Concurrently, the neutrophil count for patient P. was 42.7% (Table 3).

Monocytes as cells with phagocytic, antigen-presenting and regulatory activities may play a significant role in the development of numerous types of cancer influencing tumor growth and metastasis. In the periphery, monocyte frequency is known to correlate with inflammatory processes, and may serve as a prognostic parameter for the development of some cancers [44]. Patient R. at the first measurement revealed a slight increase in the relative number of monocytes (10.5%) compared to the control group (Table 3). However, in the CBA (Table S1), both the relative and absolute number of monocytes remained within the normal range. Given the heterogeneous nature of mature monocytes, which can be divided into three subpopulations (classical $CD14^{high}CD16^{-}$, non-classical $CD14^{low}CD16^{high}$ and intermediate $CD14^{high/mid}CD16^{+}$)

Table 3 Characteristics of some myeloid cell populations measured by flow cytometry (Panel №3), in the blood and adenoma tissue of two patients: patient P with primary disease, and patient R, who experienced a relapse

	Reference Intervals, Blood, %, *n* = 5	Patient P., blood, %	Patient R., blood October 2023, %	Patient R., blood February 2024, %	Patient R., blood April 2024, %	Patient P., adenoma, %	Patient R., adenoma October 2023, %	Patient R., adenoma April 2024, %
CD45 + CD14 + monocytes	7.2–9.1	8.73	10.5 >	7.06	8.73	20.5	10.8	12.3
$CD14^{high}CD16$- classical monocytes	90.8–95.5	90.4	96	97.2	92.7	15.3	58.5	3.49 <
$CD14^{high/mid}CD16$ + intermediate monocytes	2.3–5.0	4.14	2.96	1.21	3.76	67.8 >	31.4 >	21.3 >
$CD14^{low}CD16^{high}$ non-classical monocytes	1.9–4.2	4.62	0.79 <	1.48	3.35	14.1 >	10,6 >	75.2 >
CD14 + CD11b + HLA-DR + ^{high} monocytes	7.6–14.1	11.9	8.67	7.06	9.31	70.1 >	35.7 >	94 >
CD14 + CD11b + HLA-DR-/ + ^{med} monocytes	85.6–91.5	87.3	90.4	92.5	90.5	24.5	61.9	2.97
CD45 + CD16 + neutrophils	42.7–52.5	42.7	53.4	19.3 <	50.2	NA	NA	0.87
M-MDSC out of CD45 + leukocytes	0.0007 –0.09	0.38 >	0.8 >	0.14	0.19	NA	0.09	0.02
PMN-MDSC out of CD45 + leukocytes	0—0.002	0	0.0007	0.0005	0.008	0	0	0

Notations: > strong overperformance; < underperformance

in humans, an additional evaluation of these subpopulations was conducted. In patient R. at the time of admission in October 2023, a slight decrease in the frequency of non-classical $CD14^{low}CD1^{6high}$ monocytes was observed up to 0.79% (Table 3). The level of HLA-DR expression on the patients' monocytes remained within the normal range (Table 3).

Peripheral MDSCs are a group of immature monocytes and neutrophils undergoing pathological activation contrary to that of terminally differentiated mature myeloid cells [45]. These cells typically serve a regulatory and frequently immunosuppressive function in the immune response to tumors. Currently, two major subpopulations of MDSCs are identified based on their phenotype and morphology: polymorphonuclear (PMN-MDSCs) with a CD11b + CD14-CD15 + phenotype and monocytic (M-MDSCs) with a CD11b + CD14 + CD15- phenotype. MDSCs are not typically present in the peripheral blood of healthy individuals or with concentrations typically below the limit of detection. According to our data the frequency of these cells in peripheral blood of healthy donors was no greater than 0.1% of all leukocytes (Table 3). In various malignant neoplasms, myelopoiesis is activated and an increase in MDSCs in the blood is observed [46]. Furthermore, an excess of M-MDSCs was observed in the examined patients in comparison to the reference group of healthy volunteers. Moreover, patient R. at her first relapse experienced a higher percentage of M-MDSCs than patient P. (0.8% and 0.38%, respectively; Table 3). It is notable that then the level of M-MDSCs in patient R. demonstrated a decline over the period of observation, though it remained a little higher than the reference values. It is also interesting that only this particular type of MDSC was observed in the blood, while the level of PMN-MDSCs remained practically unchanged. MDSCs have been demonstrated to correlate with adverse outcomes in numerous tumor types [47, 48]. Additionally, it is worthy of note that M-MDSCs exhibit a greater capacity to stimulate dormant metastatic cells in comparison to PMN-MDSCs [48].

PitNETs: myeloid cells and myeloid suppressors (panel №3)

Mononuclear myeloid cells within tumors likely exist at different phases of differentiation, ranging from monocytes and M-MDSCs to macrophages. TME exerts a profound influence on the frequency and phenotype of monocytes. Distinguishing between monocytes recruited to the tumor, macrophages of monocytic origin or tissue-resident macrophages is challenging and requires the elaboration of a more comprehensive cytometric panel

of antibodies. Nevertheless, the data obtained from our two panels (№3 & 4) for myeloid cells were sufficient for interpretation. The gating strategy undertaken at the cytometric analysis of myeloid cells in PitNET samples is demonstrated in Fig. S6.

The percentage of CD45 + CD14 + monocytes (or monocytes/macrophages) in patient P. was higher than that in patient R., with a value of 20.5% compared to 10.8% and 12.3% at two different measurements for patient R., respectively (Table 3). It is noteworthy that the ratio of monocyte subpopulations in the PitNET samples exhibited a distinct profile compared to that observed in the blood. The proportion of classical $CD14^{high}CD16^{-}$ monocytes, that constitute the predominant monocyte subpopulation in the blood and typically secrete proinflammatory cytokines, possess high phagocytic activity as well as capacity to produce reactive oxygen species (ROS), decreased in PitNET samples of the patients. Their frequency dropped to 15.3% in patient P., while in patient R. it equaled 58.5% and 3.49%, respectively (Table 3). We observed that the proportion of CD16 + expressing monocytes in the PitNETs increased, particularly in patient R., where the relative number of non-classical $CD14^{low}CD16^{high}$ monocytes reached 75.2% at the second measurement. This demonstrates that expression level of CD16, an essential protein for antibody-dependent cellular cytotoxicity in human monocytes, was modified with disease progression. In humans, CD16-expressing monocytes have the capacity to exert cytotoxic effects in the presence of specific antibodies, thereby facilitating the destruction of tumor cells [49]. It was also notable that the proportion of monocytes with high levels of HLA-DR expression, a trait typically associated with CD16 + monocytes [50], was elevated in PitNETs relative to blood. Their proportion reached 70.1% in patient P., while in two subsequent measurements in patient R. it equaled 35.7% and 94%, respectively (Table 3).

MDSCs infiltrating tumors are thought to originate from monocytes and serve as primary agents of immunosuppression within tumor tissue. Yet, the isolation of a sufficient number of these cells from human biopsy specimens for the further analysis remains a significant challenge. The number of MDSCs is typically so low that it may be at the limit of instrument detection capacity. When measuring FMO-control containing antibodies to all antigens except CD14 to evaluate false-positive events and calculate the sensitivity level of the instrument, we detected no positive events in the target gate per 200 000 CD45 + events. This supported that our instrument sensitivity was very high, and the low values for M-MDSCs numbers we obtained were true. Therefore, the levels of M-MDSCs identified in the PitNETs, and which were lower than those observed in the blood of healthy volunteers, could suggest the potential presence of MDSCs in the PitNET of patient R, with percentages of 0.09% and 0.02% at first and second relapse, relatively (Table 3). The percentage of infiltrating leukocytes in Patient P. was too low to estimate a statistically reliable number of M-MDSCs.

PitNETs: monocytes and macrophages (Panel №4)

The gating strategy undertaken at the cytometric analysis of macrophages in PitNETs is shown in Fig. S7. Monocytes represent the primary source of tumor-associated macrophages (TAMs) that in response to various stimuli of TIME polarize towards two distinct subgroups exhibiting phenotypic and functional differences. These are classically activated macrophages (M1) and alternatively activated macrophages (M2). M1 macrophages with a CD163-CD206- phenotype have anti-tumour activity and are capable of secreting a number of pro-inflammatory cytokines (e.g. (e.g. IL-1β, IL-6, TNF-α). M2 macrophages with CD163 + CD206 + phenotype possess immunosuppressive properties and are capable of producing ECM components, angiogenic factors, IL-10, and TGF-β. They are associated with tumor development, metastasis, and poor prognosis [49, 51]. The frequency of macrophages among all cell types of PitNETs including tumor cells, stromal cells and leukocytes were higher in patient R. at both relapses than in patient P. (Fig. 3, f1, Table 4). But among leukocytes the frequency of macrophages was opposite: we observed 29.4% macrophages with $CD45^{+}CD64^{bright}CD11b^{low}$ phenotype among leukocytes infiltrating the pituitary tissue of patient P. In contrast, the frequency of TAMs in patient R. was significantly lower, reaching 3.1% at the time of the first recurrence and 14% at the time of the second recurrence (Table 4). We estimated the ratio of M2/M1 macrophages from the general $CD45^{+}CD64^{bright}CD11b^{low}$ macrophage subpopulation, which was 12.5 in patient P and 13.5 in patient R at the first relapse. At the second relapse, which occurred six months later, the ratio increased dramatically to 60.8, indicating a predominance of M2 macrophages and a further reduction in the already limited number of M1 macrophages (Table 4). Furthermore, a comparison of MFI revealed an increase in CD163 expression at the second relapse. It is also noteworthy that patient P. exhibited a considerable proportion of CD206 + CD163- macrophages, comprising 40% of the total macrophage population. In contrast, patient R. displayed a prevalence of CD206-CD163 + macrophages, accounting for 30.5% of the initial measurement—Fig. 3, f2, Table 4.

The expression level of CD80, a T-cell co-stimulatory molecule, was observed to be low in M1 macrophages, with a percentage of 7.14% in patient P. and 0% and

Table 4 Relative number of macrophages and monocytes in the PitNETs of patients

	Patient P., PitNET, %	Patient R., PitNET October 2023, %	Patient R., PitNET April 2024, %
Percentage of myeloid cells infiltrating PitNET (out of all events)	0.36	1.17	4.93
$CD64^{bright}CD11b^{low+}$ macrophages from all CD45 + leukocytes	29.4	3.1	14.3
Ratio Lymphocytes/Macrophages	1.05	20.5	3.5
CD206 + CD163 + M2 macrophages	57.8	61.8	83.3
CD206 + CD163 + CD14 +	100	88.9	99.9
MFI (CD163)	4211	7126	70,707
CD206-CD163 + M2 macrophages	0	30.5	14.4
CD206 + CD163- M2 macrophages	40	3.05	0.88
CD206-CD163- M1 macrophages	4.64	4.58	1.37
CD206-CD163-CD80 +	7.14	0	5.36
CD206-CD163-CD14 +	64.3	83.3	77.8
ratio M2/M1	12.5	13.5	60.8 >
$CD64^{bright}CD11b^{high+}$ monocytes	17.7	10.4	0.5

Notations: > strong overperformance; < underperformance

5.36% in patient R. at two measurements (Table 4). It is also notable that all M2 macrophages in both patients expressed CD14 +, indicating that they likely originated from the monocytic rather than the tissue-resident compartment. The majority of M1 macrophages also expressed CD14 (Table 4).

Additionally, we analyzed $CD64^{bright}/CD11b^{high}$ subpopulation, which we designated as monocytes due to their positioning within the monocyte region on CD11b/CD64 dot plot in the blood, by CD163 and CD206 expression. All samples tested were negative by CD206, but positive for CD163. It is noteworthy that patient P. exhibited a considerable number of monocytes, accounting for 17.7% of the total leukocytes. In two separate measurements, the percentage of monocytes in patient R was 10.4% and 0.5%, respectively (Table 4).

Discussion

There is no doubt that various populations of infiltrating immune cells from both innate and adaptive immunity play critical roles in tumor growth control [35]. These include myeloid suppressor cells, macrophages, dendritic cells, NK and NKT cells, as well as T and B cells. These populations are highly heterogeneous, containing subpopulations with either pro-tumor or anti-tumor activity. Numerous studies on the role of immunocompetent cells in anti-tumor immunity suggest that the cellular composition of the TIME can vary even among patients with the same type of tumor, highlighting the complexity of molecular and cellular crosstalk, which might influence tumor behavior [29].

Any tumor is a systemic disease that transforms not only its local microenvironment but also induces changes in the broader systemic environment. Tumors are often associated with destabilization of hematopoiesis, characterized by increases in neutrophils, eosinophils, and monocytes in the periphery, and decreases in dendritic cells (DCs), B cells, and T cells [37]. Elevated peripheral neutrophil levels and a high neutrophil-to-lymphocyte (N/L) ratio are often linked to poor prognosis in patients with various cancers [52]. In PitNETs and cases of acromegaly, an increased N/L ratio is also observed [53]. We also observed this phenomenon in our patients, particularly in a patient with a recurrence of somatotropinoma, as shown in their CBA (Table S1). Post-surgery, the ratio of leukocyte subpopulations normalizes, consistent with the immune system's plasticity and ability to regenerate after tumor resection, as observed in mouse cancer models [54], and as we noted in patient R.'s blood analysis of lymphocyte subpopulations during relapse (Table 1) over six months between surgeries.

Using FC, we analyzed circulating and infiltrating lymphoid and myeloid cell subpopulations in the PitNETs, using four different antibody cocktails, developed and validated earlier (unpublished data). In the periphery of the patient with a tumor relapse, we observed disruptions in the homeostasis of T, B, and NK cells, with a decrease in T-cell numbers due to an increase in B and NK cells (Fig. 2, a1-a3). Both patients showed an excess of cytotoxic CD8 + T cells and a decrease in the IRI. The first relapse in patient R. was associated with a lower

frequency in CD3+CD8+lymphocytes compared to patient P. As the relapse progressed, the IRI continued to decrease, with an excess of CD8+T cells over CD4+T cells growing (Fig. 2, b1, Table 1). Additionally, during relapse, circulating CD4+and CD8+T cells expressing PD-1 increased, indicating functional exhaustion of T cells—Fig. 2, b4-b5. The number of activated CD4+CD25+T cells was elevated in both patients, suggesting an activation of the anti-tumor immune response, more pronounced in patient P. We also observed higher levels of HLA-DR+lymphocytes among total CD3+T-cells and CD3+CD8+subpopulation in patient P (Table 2). As the disease progressed in patient R., the relative number of effector CD16+CD56+NK cells decreased, while the proportion of immature CD16-CD56- NK cells increased. In patient P., the balance of these subpopulations remained normal. In the patient with tumor relapse, we also detected a reduction in the granule-mediated cytotoxic potential of CD8+T cells for perforin (Fig. 2, e1), and particularly granzyme B (Fig. 2, e2), and a similar reduction in NK cells for granzyme (Fig. 2, e4, e6, Table 2). Previous studies have reported that invasiveness in non-functioning pituitary adenomas (NFPAs) is accompanied by a decrease in CD3-CD56+NK cells, as seen in the first relapse of patient R., as well as a significant increase in CD3+CD8+CD28-(CD8+Tregs) and IL-10 in the periphery [55].

The number of leukocytes infiltrating PitNETs can be an important prognostic factor. TILs and TAMs are the most studied components of the TIME in PitNETs [31, 32]. During surgery for the first relapse in patient R., 7.42% of TILs were found in the surgical material among all cells, representing 23.4% of all lymphocytes among leukocytes (Table 1). After the second relapse and surgery, the number of TILs increased to 28.2% across PitNET cells with 50.9% of lymphocytes. In patient P., the percentage of TILs was 30.2% of all leukocytes. While high leukocyte infiltration is generally considered a favorable prognostic indicator for survival, the specific composition of leukocyte subpopulations, especially lymphocytes, may play a crucial role.

TILs are phenotypically and functionally heterogeneous. Cytotoxic CD8+T cells, CD8+memory T cells (CD8+CD45RO+), CD4+T helper type 1, innate cytotoxic lymphocytes, and CD56+NK cells are typically considered antitumor cells, capable of directly interacting with tumor antigens to initiate cytotoxic responses [24, 35, 56]. Conversely, other TILs, such as CD4+T helper types 2 and 17, and CD4+CD25+FoxP3+regulatory T cells, exert protumorigenic effects by inhibiting effector lymphocytes, which is unfavorable for the patient [27, 57, 58]. PitNETs are known to be infiltrated by CD3+, CD8+, CD4+, FoxP3+, CD45RO+, and CD56+cells. When compared with normal pituitary tissue, PitNETs contain more CD4+T cells and fewer CD8+T cells, leading to a two-fold decrease in the CD8/CD4 ratio [24]. The expression of tumor-infiltrating CD3+and CD4+lymphocytes is higher in hormonally active pituitary tumors compared to hormonally inactive ones. Additionally, the expression of CD3, CD4, CD8, and CD45 is higher in tumors with elevated Ki-67 levels [7]. While CD45+infiltration is consistent across different PitNET subtypes, CD4+and CD8+expression strongly correlates with elevated GH levels. Poor clinical prognosis is often associated with CD45 expression [6]. In somatotropinomas, CD8+lymphocyte infiltration is significantly lower in tumors with cavernous sinus invasion and in tumors resistant to first-generation somatostatin analogs [33]. In the study by Lu JQ et al., CD4+and CD8+T cell infiltration in pituitary tumors was relatively sparse, but somatotropinomas contained significantly higher levels of both CD4+and CD8+T cells compared to corticotropinomas. Moreover, densely granular somatotropinomas had more CD4+T cells than corticotropinomas and more CD8+T cells than null-cell pituitary tumors. However, no correlation was found between CD4+T cell counts and tumor size or invasiveness [29]. In a separate study by Sato M. et al., assessing FoxP3+T cells in hormonally inactive pituitary tumors, a higher FoxP3/CD8 ratio was noted in the invasive tumor group, further suggesting the role of regulatory T cells in tumor progression [59].

We do not have data on the composition of TILs for patient R. at the initial diagnosis. However, we believe it is affordable to assess the dynamics of the immune response on the basis of the material from two relapses. With tumor progression in the pituitary tissue and after multiple traumatic surgical interventions in patient R., her TIME differed significantly from that of patient P. T cells were the predominant lymphocyte population in patient P, whereas in patient R. T cells were also predominant after the first relapse surgery—Fig. 3, a1. However, following the second relapse surgery, NK cells became predominant, accounting for 57% of the lymphocyte population—Fig. 3, a3. Among NK cells, a high percentage were cytokine-producing CD16-CD56+NK cells—Fig. 3, a4. In patient P., the ratio of cytotoxic CD8+T cells to CD4+T cells was three times higher. On the contrary, patient R. had an extremely low percentage (3.72%) of cytotoxic CD8+CD4- T cells among CD3+T cells upon admission with the first relapse (Table 1). Additionally, after relapse, CD4+CD8+DP T cells appeared in significant numbers (36.8%), though their proportion decreased in subsequent measurements (Fig. 3, b1, Table 1). These DP cells often arise from CD4+T cells, which secondarily acquire CD8+characteristics under conditions of

persistent tumor antigen stimulation. Although the emergence of such DP cells has been observed in TILs across various cancers [40], we have not previously encountered their presence in PitNETs. Additionally, the number of T lymphocytes expressing the activation molecule CD38 was significantly lower in patient R., who had a more aggressive disease course. However, over time, there was an increase in the number of activated CD3 + CD38 + and CD8 + CD38 + cells within the PitNET tissue (Table 2). The expression of the HLA-DR molecule was comparable between the two patients.

The second recurrence of the PitNET in patient R. was marked by a significant increase in the expression of the regulatory molecule PD-1 on CD4 + and CD8 + T cells (Fig. 3, b4-b5, Table 1). It is well known that the interaction between PD-1 and its ligand PD-L1 plays a critical role in modulating T cell activity and enabling tumor immune evasion. PD-1, a transmembrane receptor expressed on the surface of many immune cells, is classified as an immune checkpoint molecule. During early T cell activation, PD-1 primarily influences effector function by weakening the activation signal from TCR and CD28, without inducing functional exhaustion. However, with chronic stimulation, such as from a persistent tumor antigen, prolonged PD-1 expression can lead to T cell exhaustion [41, 60]. High PD-L1 expression is commonly observed in somatotropinomas, particularly in sparsely granulated somatotropic pituitary tumors, which tend to exhibit more aggressive behavior [61]. Somatotropinomas with high PD-1/PD-L1 expression often display aggressive clinical behavior, despite high levels of CD8 + T cell infiltration, suggesting diminished functional activity of CD8 + T cells [62].

We did not detect Tregs in the adenoma of patient P. However, they were present in high numbers in patient R., with measurements showing 34.8% and 19.4% in two instances (Fig. 3, c1). Tregs are crucial for constraining the immune response and preventing tissue damage from excessive T-cell activation [63]. A high infiltration of Tregs and a reduction in CD8/Tregs ratio are often associated with poor prognosis in various cancers [64]. In the adenoma of the patient R. with relapse, we observed a decrease in the CD8/Treg ratio, dropping to 0.1 in the first measurement and rising to 1.23 in the second. Interestingly, the proportion of Tregs expressing PD-1 was notably high, reaching 91% after the second relapse (Table 1). It is known that PD-L1 binding to PD-1 on T cells promotes their conversion into Tregs [65]. In TIME, PD-L1 expression often correlates with increased numbers of intratumoral FoxP3 + Tregs, consistent with its role in maintaining FoxP3 expression in CD4 T cells and stimulating the polarization of naïve CD4 T cells into Tregs. Furthermore, PD-1 expression in Tregs inactivates asparaginyl endopeptidase, stabilizing FoxP3 expression and maintaining Treg function [66].

In addition to analyzing tumor-infiltrating T cells, we also assessed tumor-infiltrating B and NK cells. The peripheral blood of patient R. at the first measurement revealed a significantly high percentage of B cells (38.3%), correlating with the increased presence of B cells in her adenoma (11.3%) (Figs. 2, a2 and 3, a2, Table 1). Disease progression was further accompanied by the sustained reduction of B-cells along with the increase of T—and NK-cells number. Even after normalizing the TBNK cell balance, the number of B cells in patient R. remained higher than in patient P. (Fig. 2, a2). Tumor-infiltrating B cells may play a key regulatory role in tumor development, but their role is controversial that can be explained by their functional heterogeneity [67]. As antigen-presenting cells, B cells can stimulate tumor-specific T cell expansion and contribute to the antitumor response, possibly producing antibodies against the tumor. Conversely, regulatory B cells (Bregs) can suppress antitumor immunity by inhibiting T cells, dendritic cells, and macrophages through cytokines like IL-10, IL-35, and TGF-β. Notably, in the second measurement in patient R., the proportion of PD-1-expressing B cells increased to 10.1% (Table 1).

NK cells are key effector cells in innate immunity, capable of recognizing and eliminating aberrant tumor cells [68]. Their role in both the tumor macro- and microenvironment warrants further investigation due to their functional heterogeneity and complex activation states. NK cells recruited to tumors often undergo phenotypic changes into regulatory CD56 + cells. In patient P., cytokine-producing regulatory CD16-CD56 + NK cells accounted for 53.1%, while in patient R., they made up 66.6% during the second relapse (Fig. 3, a4, Table 1). The overall percentage of CD3-CD20- NK cells and CD3-CD56 + NK cells was low in patient R. at the first measurement (5.57% and 2.54%, respectively) but sharply increased after six months to 57% and 48.6% (Fig. 3, a3, Table 1). Additionally, the proportion of CD8 + CD38 + NK cells in patient R. during the second relapse reached 10.7%, comparable to 8.82% in patient P. (Table 2). It's worth noting that CD3-CD56 + CD8 + NK cells may possess memory-like properties [69]. NK cells are capable of "remembering" their cytokine environment, and under similar conditions, they may differentiate into memory NK cells [68]. The TIME can provide conditions for long-term priming of NK cells with cytokines, facilitating this differentiation [70]. Interestingly, the pituitary tissue of patient P. had a higher proportion of NKT cells compared to patient R.

It's worth adding that both patients were of significantly distinct age, reaching 20 and 63 years, which potentially

could contribute to the difference in immune cell composition between the patients due to immune aging. Age-related immune changes in blood usually comprise decline in CD4+and CD8+T-cells as well as B-cells, whereas the numbers of NK-cells and regulatory T-cells are increased. Also, a reduction of naïve lymphocytes is a hallmark of an immune system aging. At the same time it is known, that lymphocyte subsets are characterized of high inter-individual variations, and change at relative stable rates in a highly individualized manner [39]. In our study we observed the higher frequency of naïve cells in blood of the younger patient R. (Fig. 2, b2-b3, Table 1), which could be associated with age. On the contrary, we detected higher number of CD4+T-cells in the older patient P. The same trend was for CD8+T-cells if compared to the first relapse of the patient R, with further increasing the number of CD8+T-cells. In both patients the number of CD8+T-cells were higher than in healthy donors, with concomitant reduction in CD4+T-cells (Fig. 2, b1, Table 1), which is often associated with tumor [79]. Tumors and tumor-associated antigens could be a driving force for the increase of memory T-cells. Though it appeared difficult to register it in blood, the majority of CD4+and CD8+T-cells were of memory phenotype in the PitNETs samples, which we suggest, rather indicates tumor-specific role of these cells.

The cytotoxic potential of CD8+T cells and NK cells is partly mediated by their ability to produce cytolytic granules containing granzyme B and perforin [71]. Granzyme B induces apoptotic cell death, while perforin can additionally cause osmotic lysis and necrotic cell death. In the patient with a more aggressive disease course, the number of effector cells producing perforin and granzyme B, including those co-expressing both proteins, was significantly lower both in the periphery and in the tumor (Figs. 2 and 3, d1-d2, Table 2). Even though by the time of the second relapse, NK cells made up more than 50% of all TILs in the TIME of this patient, most of which had the CD3-CD56+phenotype, only 6% of CD56+lymphocytes in patient R. were capable of exerting cytotoxicity via perforin production. Similarly, CD16+cells in this patient had limited perforin-mediated cytotoxic potential. In contrast, 66.6% of CD16+lymphocytes and 29% of CD56+cells could exert cytotoxicity via perforin in patient P. (Fig. 3, e3, e5, Table 2). Comparable perforin expression levels were observed in CD8+cells in both patients (Fig. 3, e1, Table 2). The aggressive tumor course in patient R. was marked by lower infiltration of CD16+and CD56+effector cells capable of exerting cytotoxicity via granzyme B at the first relapse, with this potential decreasing further to 18% and 8% by the second relapse (Fig. 3, e4, e6, Table 2).

In addition to lymphoid cells, we also analyzed several myeloid cell populations in both blood and adenoma. Tumor-associated myeloid cells are found among the most abundant cells in the TME, accounting for up to 50% of the total tumor mass in solid tumors [72]. The TIME of tumors often contains monocytes, MDSCs, as well as tumor-associated DCs and macrophages, into which monocytes can differentiate under TIME conditions. Monocyte differentiation depends on the cytokine network and other TIME factors, and it is currently not fully understood what exactly influences the differentiation of monocytes into immunosuppressive macrophages rather than immunostimulatory DCs, as well as into MDSCs [44]. The proportion of CD45+CD14+monocytes in patient R. in PitNETs in both cases was lower than in patient P. (Table 3). In both patients, the ratio of monocyte subpopulations in the PitNETs was different from the blood with a predominance of the proportion of CD16+expressing monocytes. In patient P., intermediate $CD14^{high/mid}CD16+$monocytes predominated (67.8%), and in patient R., at the time of the first relapse, classical proinflammatory $CD14^{high}CD16^{-}$ monocytes prevailed (58.5%), while at the time of the 2nd relapse, non-classical $CD14^{low}CD16^{high}$ monocytes were in abundance (75.2%) (Table 3). The latter are attributed to the function of tissue macrophages in the blood [73]. In humans, monocytes with CD16 on their surface have the ability to be cytotoxic in the presence of certain antibodies. These monocytes can destroy primary leukemia cells, tumor cells, and cells infected with the hepatitis B virus [49]. It is interesting to note that in patient P., a high density of HLA-DR molecule expression was detected in 70.1% of monocytes. Whereas in patient R. the frequency of monocytes with a high density of HLA-DR increased sharply with the disease progression, reaching 35.7% at the time of the first relapse, and 94% at the time of the second relapse.

However, it is very difficult to distinguish monocytes from macrophages in tissue. In most cancers, TAMs appear as a result of differentiation of monocytes infiltrating from blood into tumor under the influence of cytokines and chemokines secreted by tumor cells [44]. Macrophages are described as one of the most common cells in TIME PitNETs. It is noted that they can correlate with the tumor size and its invasiveness [32]. Patient R. had higher infiltration of macrophages into PitNET tissue compared to patient P., with their number increasing on disease progress (Fig. 3, f1, Table 4). It supports the previous reports on the positive correlation of CD68+macrophage infiltration with invasive behavior of PitNETs, with macrophages detected via immunohistochemistry [32, 80]. It's worth noting that when analyzing TAM

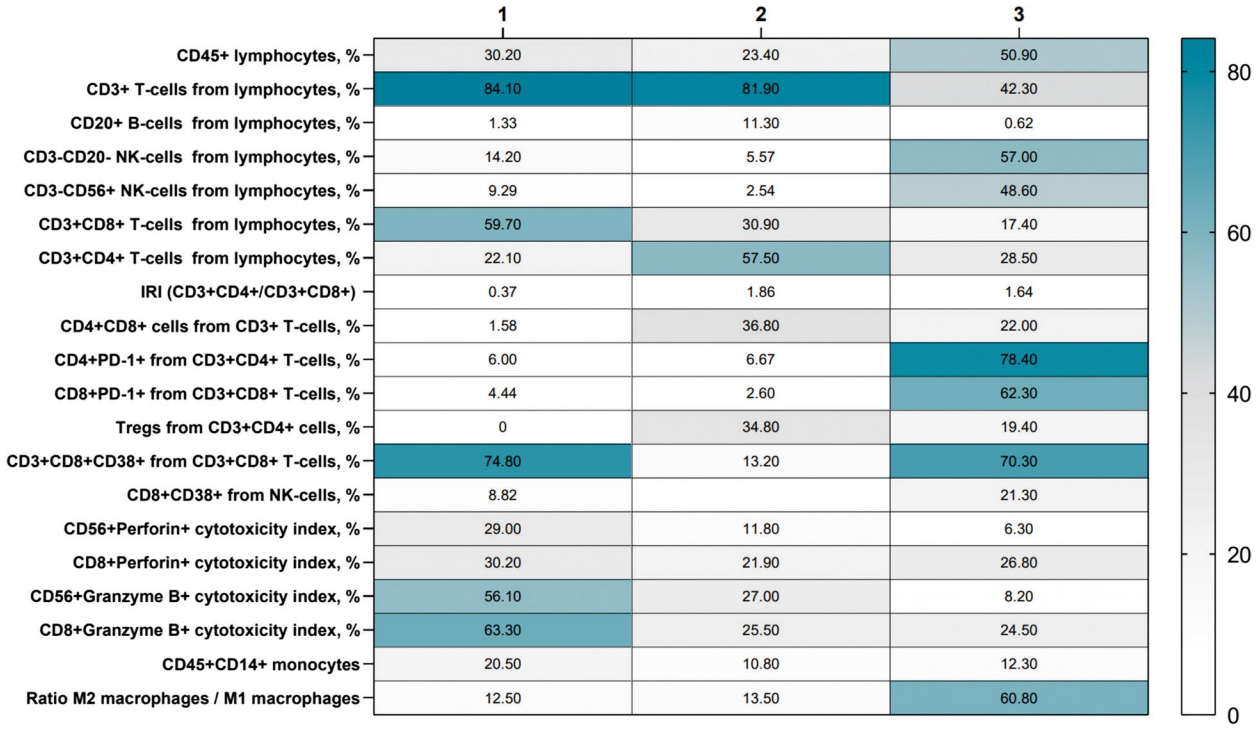

Fig. 6 The heatmap depicts the frequencies of various lymphoid and myeloid cell subpopulations infiltrating the somatotropinomas of patient P. (1st column) and patient R. at the time of the first relapse in October 2023 (2nd column) and the second relapse in April 2024 (3rd column)

frequency among leukocytes, we observed the opposite relations: more macrophages were in patient P. The ratio of lymphoid and myeloid cells among all CD45 + leukocytes can be another crucial prognostic parameter in PitNETs. In patient P. the ratio of lymphocytes to macrophages was nearly equal. In contrast, in patient R. at the initial measurement in October 2023, lymphocytes outnumbered macrophages with a ratio of 20.5. Six months later, there was a notable increase in the proportion of macrophages, accompanied by a decline in lymphocytes, resulting in a ratio of 3.5 (Table 4). Immunosuppressive TAMs promote tumor growth, support angiogenesis, inhibit the activity of cytotoxic CD8 + T cells, and recruit immune cells with suppressive activity—Tregs, MDSCs—to TIME [74]. The ratio of M2 and M1 macrophages, arisen due to the presence of certain macrophage-activating factors in TIME, can be an indicator of immunosuppression. It was 12.5 in patient P. and 13.5 in patient R. at the first measurement, and six months later this ratio in patient R. increased sharply to 60.8, demonstrating the worsening of the immunosuppressive background (Fig. 3, f2, Table 4). Moreover, most M1 macrophages were negative for the expression of CD80, a molecule that co-stimulates T cells.

Depending on the activation stimulus, a wide spectrum of mixed and functionally distinct macrophages may be present in the tumor, the poles of which are M1 and M2 types of macrophages [75]. M2 macrophages themselves are also functionally very heterogeneous, demonstrating a spectrum of different activation states and functional capabilities. In the present work, we identified M1 and M2 macrophages by the expression of CD206 and CD163 markers. Positive expression of CD206 (C-type mannose receptor) and CD163 (Hemoglobin-Haptoglobin Scavenger Receptor) is considered a sign of M2 macrophages. CD206 expression on macrophages is increased in response to IL-4, TGF-β, GM-CSF (granulocyte macrophage colony-stimulating factor), while CD163 expression is increased in response to M-CSF, IL-6, IL-10, and glucocorticoids and decreased in response to TNF-α, TGF-β, IFN-γ, and LPS. Macrophages co-expressing CD206 and CD163 are the source of high levels of IL-10, IL-1ra, and CCL18 in TIME [75], which contribute greatly to the immunosuppressive background in TIME. In the relapsed patient, we note a high proportion of M2 macrophages expressing both CD206 and CD163, 61.8% and 83.3% in 2 measurements. Moreover, at the 2nd measurement in April 2024, we note a sharp increase in the expression level of CD163, which correlates with the data from other studies on the increase in the level of CD163 in M2 macrophages under the influence of tumor factors [76]. It is also interesting that in patient P., a large

subpopulation of CD206 + CD163- macrophages was noted, accounting for 40%, while in patient R. at the 1st measurement, 30.5% of CD206-CD163 + macrophages. These subpopulations are also subpopulations of M2 macrophages, reflecting the continuum of different TIME factors leading to different subtypes of M2 macrophages.

MDSCs are pathologically activated monocytes and neutrophils with immunosuppressive properties. Their increased number is often observed in the systemic circulation due to aberrant myelopoiesis in conditions of chronic inflammation, autoimmune diseases and tumor processes [45]. There is a correlation between the number of MDSCs in the periphery and an unfavorable clinical outcome [47] in various malignant neoplasms and with resistance to therapy [77]. In the local TME, M-MDSCs can be formed as a result of differentiation of monocytes recruited to TIME, which, under the influence of many TIME factors, change their transcriptional and post-transcriptional profile and acquire immunosuppressive properties [78]. We observed an increase in M-MDSCs in the examined patients compared to the reference group of healthy volunteers both in the blood and in the adenoma, and in the patient with a relapse in the blood we detected higher values of M-MDSCs, amounting to 0.8%, and in patient P—0.38% (Table 3). We also find M-MDSCs in the adenoma of patient R., the proportion of which was 0.09% and 0.02% (Table 3) in 2 measurements, respectively.

Thus, myeloid cells, which are represented in the TIME by monocytes migrating into the tumor and capable of differentiating into tumor-associated macrophages, dendritic cells, and MDSCs, play a crucial role in establishing and maintaining an immunosuppressive TIME. Immunotherapies that target macrophages, reducing their number, survival, and proliferative activity, have been shown to enhance the anti-tumor activity of T cells [44]. Consequently, an important parameter to consider is the ratio of lymphoid to myeloid cells among all CD45 + leukocytes. Interestingly, in patient R., lymphoid cells predominated over myeloid cells at the time of relapse (Table 4), though the proportion of lymphoid cells decreased over the course of six months. Another critical factor is infiltration of leukocytes into adenoma tissue. In this context, patient R. exhibited a higher proportion of CD45 + infiltrating leukocytes, which aligns with earlier findings suggesting a correlation between adenoma size and the number of infiltrating immune cells [32].

Here, through multicolor FC, we conducted a quantitative analysis of the TIME in two cases of somatotropinoma. We compared lymphocyte subpopulations and assessed their cytotoxicity and activation potential. In addition, we evaluated the infiltration of somatotropinomas by monocytes, M1 and M2 macrophages, and myeloid suppressors. Our analysis suggests that the patient with relapse displayed a more immunosuppressive profile across a number of parameters (Fig. 6). The differences in TIME between the two patients, despite sharing the same diagnosis, likely contributed to their differences in disease progression. However, due to the absence of material from patient P. at the time of diagnosis prior to relapse and given that the data are based on only two patients, it is difficult to identify which immune parameters may predict relapse. Nonetheless, our findings provide a foundation for future large-scale studies of TIME in somatotropinomas with multicolor FC, with the goal of identifying immunological biomarkers for relapse. Understanding the balance between effector and suppressor populations of lymphoid and myeloid cells, both in systemic and local immunity, could pave the way for personalized treatment approaches for patients with PitNETs in the future.

Abbreviations

CBA	Clinical blood analysis
CI	Cytotoxicity index
DN	Double negative
DP	Double positive
FC	Flow cytometry
IRI	Immunoregulatory index
MRI	Margentic resonance imaging
PD-1	Programmed cell death protein 1
TAMs	Tumor-associated macrophages
TCR	T-cell receptor
TILs	Tumor-infiltrating lymphocytes
TIME	Tumor immune microenvironment
Tregs	Regulatory T-cells

Supplementary Information

The online version contains supplementary material available at https://doi.org/10.1186/s12902-025-01865-9.

Supplementary Material 1.

Supplementary Material 2 Table S1.

Acknowledgements
NA

Clinical trial number
Not applicable.

Authors' contributions
M.L., D.L., E.P., L.K.D were engaged in conceptualization; A.G., V.A.—performed surgery M.L. and E.Z. were responsible for flow cytometry methodology, panel design and cytemeter settings; M.L., E.Z., V.M., A.S. and L.U.D. performed analysis of flow cytometry files; V.M., M.L. performed flow cytometry measurements; D.L., M.L.—prepared the original draft; D.L.,M.L, V.M., E.P., E.Z.. review and edited the draft; A.S., L.U.D., E.P. made technical visualization; M.L., G.M., N.M., S.R., V.C.—supervised the project; V.C., N.M.— funding acquisition.

Funding
This research was funded by the Ministry of Science and Higher Education of the Russian Federation (agreement No. 075–15-2022–310 from 20 April 2022).

Data availability
The fully anonymized data of CBA are available in Supplementary file. The raw flow cytometry files as fcs-files are digitally stored with virtual database of Endocrinology Research Centre, Moscow, Russian Federation and will be available upon acceptance. For access to the database contact to Marina Loguinova, e-mail: Loginova.Marina@endocrincentr.ru; marina.loguinova@mail.ru.

Declarations

Ethics approval and consent to participate
The study was conducted in accordance with the Declaration of Helsinki and approved by the Local Ethics Committee of the Endocrinology Research Centre (Approval No. 17, dated 27 September 2023).

Consent to publication
Written informed consent for publication of the patients' details and/or clinical images was obtained from the patients. A copy of the consent form is available for review by the Editor of this journal.

Competing interests
The authors declare no competing interests.

Received: 12 November 2024 Accepted: 4 February 2025
Published online: 12 February 2025

References

1. Lu L, Wan X, Xu Y, Chen J, Shu K, Lei T. Prognostic Factors for Recurrence in Pituitary Adenomas: Recent Progress and Future Directions. Diagnostics (Basel). 2022;12(4):977. https://doi.org/10.3390/diagnostics12040977.
2. Villa C, Baussart B, Assié G, Raverot G, Roncaroli F. The World Health Organization classifications of pituitary neuroendocrine tumours: a clinico-pathological appraisal. Endocr Relat Cancer. 2023;30(8):e230021. https://doi.org/10.1530/ERC-23-0021.
3. Raverot G, Burman P, McCormack A, Heaney A, Petersenn S, Popovic V, Trouillas J, Dekkers OM, European Society of Endocrinology. European Society of Endocrinology Clinical Practice Guidelines for the management of aggressive pituitary tumours and carcinomas. Eur J Endocrinol. 2018;178(1):G1–24. https://doi.org/10.1530/EJE-17-0796.
4. Dai C, Liang S, Sun B, Li Y, Kang J. Anti-VEGF Therapy in Refractory Pituitary Adenomas and Pituitary Carcinomas: A Review. Front Oncol. 2021;17(11):773905. https://doi.org/10.3389/fonc.2021.773905.
5. Dekkers OM, Karavitaki N, Pereira AM. The epidemiology of aggressive pituitary tumors (and its challenges). Rev Endocr Metab Disord. 2020;21(2):209–12. https://doi.org/10.1007/s11154-020-09556-7.
6. Dai C, Liang S, Sun B, Kang J. The Progress of Immunotherapy in Refractory Pituitary Adenomas and Pituitary Carcinomas. Front Endocrinol (Lausanne). 2020;11(11):608422. https://doi.org/10.3389/fendo.2020.608422.
7. Marques P, Grossman AB, Korbonits M. The tumour microenvironment of pituitary neuroendocrine tumours. Front Neuroendocrinol. 2020;58:100852. https://doi.org/10.1016/j.yfrne.2020.100852.
8. Raverot G, Ilie MD, Lasolle H, Amodru V, Trouillas J, Castinetti F, Brue T. Aggressive pituitary tumours and pituitary carcinomas. Nat Rev Endocrinol. 2021;17(11):671–84. https://doi.org/10.1038/s41574-021-00550-w.
9. Buchy M, Lapras V, Rabilloud M, Vasiljevic A, Borson-Chazot F, Jouanneau E, Raverot G. Predicting early post-operative remission in pituitary adenomas: evaluation of the modified knosp classification. Pituitary. 2019;22(5):467–75. https://doi.org/10.1007/s11102-019-00976-6.
10. Ilie MD, Jouanneau E, Raverot G. Aggressive Pituitary Adenomas and Carcinomas. Endocrinol Metab Clin North Am. 2020;49(3):505–15. https://doi.org/10.1016/j.ecl.2020.05.008.
11. Imber BS, Lin AL, Zhang Z, Keshavamurthy KN, Deipolyi AR, Beal K, Cohen MA, Tabar V, DeAngelis LM, Geer EB, Yang TJ, Young RJ. Comparison of Radiographic Approaches to Assess Treatment Response in Pituitary Adenomas: Is RECIST or RANO Good Enough? J Endocr Soc. 2019;3(9):1693–706. https://doi.org/10.1210/js.2019-00130.
12. Nishioka H. Aggressive pituitary tumors (PitNETs). Endocr J. 2023;70(3):241–8. https://doi.org/10.1507/endocrj.EJ23-0007.
13. Li CZ, Gui SB, Zong XY, Zhang YZ. The Expression of Estrogen Receptor Subtypes in Prolactinomas and Their Relationship to Tumor Biological Behavior. Biomed Environ Sci. 2015;28(11):820–2. https://doi.org/10.3967/bes2015.113.
14. Liu X, Kano M, Araki T, Cooper O, Fukuoka H, Tone Y, Tone M, Melmed S. ErbB receptor-driven prolactinomas respond to targeted lapatinib treatment in female transgenic mice. Endocrinology. 2015;156(1):71–9. https://doi.org/10.1210/en.2014-1627.
15. Di Ieva A, Rotondo F, Syro LV, Cusimano MD, Kovacs K. Aggressive pituitary adenomas–diagnosis and emerging treatments. Nat Rev Endocrinol. 2014;10(7):423–35. https://doi.org/10.1038/nrendo.2014.64.
16. Shi C, Ye Z, Han J, Ye X, Lu W, Ji C, Li Z, Ma Z, Zhang Q, Zhang Y, He W, Chen Z, Cao X, Shou X, Zhou X, Wang Y, Zhang Z, Li Y, Ye H, He M, Chen H, Cheng H, Sun J, Cai J, Huang C, Ye F, Luo C, Zhou B, Ding H, Zhao Y. BRD4 as a therapeutic target for nonfunctioning and growth hormone pituitary adenoma. Neuro Oncol. 2020;22(8):1114–25. https://doi.org/10.1093/neuonc/noaa084.
17. Uraki S, Ariyasu H, Doi A, Takeshima K, Morita S, Inaba H, Furuta H, Fukuhara N, Inoshita N, Nishioka H, Nakao N, Yamada S, Akamizu T. MSH6/2 and PD-L1 Expressions Are Associated with Tumor Growth and Invasiveness in Silent Pituitary Adenoma Subtypes. Int J Mol Sci. 2020;21(8):2831. https://doi.org/10.3390/ijms21082831.
18. Ji Y, Vogel RI, Lou E. Temozolomide treatment of pituitary carcinomas and atypical adenomas: systematic review of case reports. Neurooncol Pract. 2016;3(3):188–95. https://doi.org/10.1093/nop/npv059.
19. Syro LV, Rotondo F, Camargo M, Ortiz LD, Serna CA, Kovacs K. Temozolomide and Pituitary Tumors: Current Understanding, Unresolved Issues, and Future Directions. Front Endocrinol (Lausanne). 2018;15(9):318. https://doi.org/10.3389/fendo.2018.00318.
20. McCormack A, Dekkers OM, Petersenn S, Popovic V, Trouillas J, Raverot G, ESE survey collaborators. Burman P;Treatment of aggressive pituitary tumours and carcinomas: results of a European Society of Endocrinology (ESE) survey 2016. Eur J Endocrinol. 2018;178(3):265–76. https://doi.org/10.1530/EJE-17-0933.
21. Minniti G, Flickinger J, Tolu B, Paolini S. Management of nonfunctioning pituitary tumors: radiotherapy. Pituitary. 2018;21(2):154–61. https://doi.org/10.1007/s11102-018-0868-4.
22. Dworakowska D, Grossman AB. Aggressive and malignant pituitary tumours: state-of-the-art. Endocr Relat Cancer. 2018;25(11):R559–75. https://doi.org/10.1530/ERC-18-0228.
23. Zhang D, Way JS, Zhang X, Sergey M, Bergsneider M, Wang MB, Yong WH, Heaney AP. Effect of Everolimus in Treatment of Aggressive Prolactin-Secreting Pituitary Adenomas. J Clin Endocrinol Metab. 2019;104(6):1929–36. https://doi.org/10.1210/jc.2018-02461.
24. Ilie MD, Vasiljevic A, Bertolino P, Raverot G. Biological and Therapeutic Implications of the Tumor Microenvironment in Pituitary Adenomas. Endocr Rev. 2023;44(2):297–311. https://doi.org/10.1210/endrev/bnac024.
25. Burman P, Casar-Borota O, Perez-Rivas LG, Dekkers OM. Aggressive Pituitary Tumors and Pituitary Carcinomas: From Pathology to Treatment. J Clin Endocrinol Metab. 2023;108(7):1585–601. https://doi.org/10.1210/clinem/dgad098. Erratum.In:JClinEndocrinolMetab.2023;108(10):e1163.doi:10.1210/clinem/dgad222.
26. Sol B, de Filette JMK, Awada G, Raeymaeckers S, Aspeslagh S, Andreescu CE, Neyns B, Velkeniers B. Immune checkpoint inhibitor therapy for ACTH-secreting pituitary carcinoma: a new emerging treatment? Eur J Endocrinol. 2021;184(1):K1–5. https://doi.org/10.1530/EJE-20-0151.
27. Balkwill FR, Capasso M, Hagemann T. The tumor microenvironment at a glance. J Cell Sci. 2012;125(Pt 23):5591–6. https://doi.org/10.1242/jcs.116392.
28. Liu S, Sun Q, Ren X. Novel strategies for cancer immunotherapy: counter-immunoediting therapy. J Hematol Oncol. 2023;16(1):38. https://doi.org/10.1186/s13045-023-01430-8.
29. Wang Z, Guo X, Gao L, Deng K, Lian W, Bao X, Feng M, Duan L, Zhu H, Xing B. The Immune Profile of Pituitary Adenomas and a Novel Immune Classification for Predicting Immunotherapy Responsiveness. J Clin

Endocrinol Metab. 2020;105(9):e3207–23. https://doi.org/10.1210/clinem/dgaa449.
30. Tapoi DA, Popa ML, Tanase C, Derewicz D, Gheorghișan-Gălățeanu AA. Role of Tumor Microenvironment in Pituitary Neuroendocrine Tumors: New Approaches in Classification, Diagnosis and Therapy. Cancers (Basel). 2023;15(21):5301. https://doi.org/10.3390/cancers15215301.
31. Chiloiro S, De Marinis L. The immune microenviroment in somatotropinomas: from biology to personalized and target therapy. Rev Endocr Metab Disord. 2023;24(2):283–95. https://doi.org/10.1007/s11154-022-09782-1. (Epub 2023 Jan 20).
32. Lu JQ, Adam B, Jack AS, Lam A, Broad RW, Chik CL. Immune Cell Infiltrates in Pituitary Adenomas: More Macrophages in Larger Adenomas and More T Cells in Growth Hormone Adenomas. Endocr Pathol. 2015;26(3):263–72. https://doi.org/10.1007/s12022-015-9383-6.
33. Iacovazzo D, Chiloiro S, Carlsen E, Bianchi A, Giampietro A, Tartaglione T, Bima C, Bracaccia ME, Lugli F, Lauretti L, Anile C, Gessi M, Colosimo C, Rindi G, Pontecorvi A, Korbonits M, De Marinis L. Tumour-infiltrating cytotoxic T lymphocytes in somatotroph pituitary neuroendocrine tumours. Endocrine. 2020;67(3):651–8. https://doi.org/10.1007/s12020-019-02145-y.
34. Gong J, Zhao Y, Abdel-Fattah R, Amos S, Xiao A, Lopes MB, Hussaini IM, Laws ER. Matrix metalloproteinase-9, a potential biological marker in invasive pituitary adenomas. Pituitary. 2008;11(1):37–48. https://doi.org/10.1007/s11102-007-0066-2.
35. Galon J, Mlecnik B, Bindea G, Angell HK, Berger A, Lagorce C, Lugli A, Zlobec I, Hartmann A, Bifulco C, Nagtegaal ID, Palmqvist R, Masucci GV, Botti G, Tatangelo F, Delrio P, Maio M, Laghi L, Grizzi F, Asslaber M, D'Arrigo C, Vidal-Vanaclocha F, Zavadova E, Chouchane L, Ohashi PS, Hafezi-Bakhtiari S, Wouters BG, Roehrl M, Nguyen L, Kawakami Y, Hazama S, Okuno K, Ogino S, Gibbs P, Waring P, Sato N, Torigoe T, Itoh K, Patel PS, Shukla SN, Wang Y, Kopetz S, Sinicrope FA, Scripcariu V, Ascierto PA, Marincola FM, Fox BA, Pagès F. Towards the introduction of the "Immunoscore" in the classification of malignant tumours. J Pathol. 2014;232(2):199–209. https://doi.org/10.1002/path.4287.
36. Giustina A, Biermasz N, Casanueva FF, Fleseriu M, Mortini P, Strasburger C, van der Lely AJ, Wass J, Melmed S. Acromegaly Consensus Group. Consensus on criteria for acromegaly diagnosis and remission. Pituitary. 2024;27(1):7–22. https://doi.org/10.1007/s11102-023-01360-1. Erratum in: Pituitary. 2024;27(1):88. https://doi.org/10.1007/s11102-023-01373-w.
37. Hiam-Galvez KJ, Allen BM, Spitzer MH. Systemic immunity in cancer. Nat Rev Cancer. 2021;21(6):345–59. https://doi.org/10.1038/s41568-021-00347-z.
38. Reichert T, DeBruyère M, Deneys V, Totterman T, Lydyard P, Yuksel F, Chapel H, Jewell D, Van Hove L, Linden J, et al. Lymphocyte subset reference ranges in adult Caucasians. Clin Immunol Immunopathol. 1991;60(2):190–208. https://doi.org/10.1016/0090-1229(91)90063-g.
39. Lin Y, Kim J, Metter EJ, Nguyen H, Truong T, Lustig A, Ferrucci L, Weng NP. Changes in blood lymphocyte numbers with age in vivo and their association with the levels of cytokines/cytokine receptors. Immun Ageing. 2016;18(13):24. https://doi.org/10.1186/s12979-016-0079-7.
40. Schad SE, Chow A, Mangarin L, Pan H, Zhang J, Ceglia N, Caushi JX, Malandro N, Zappasodi R, Gigoux M, Hirschhorn D, Budhu S, Amisaki M, Arniella M, Redmond D, Chaft J, Forde PM, Gainor JF, Hellmann MD, Balachandran V, Shah S, Smith KN, Pardoll D, Elemento O, Wolchok JD, Merghoub T. Tumor-induced double positive T cells display distinct lineage commitment mechanisms and functions. J Exp Med. 2022;219(6):e20212169. https://doi.org/10.1084/jem.20212169.
41. Blank CU, Haining WN, Held W, Hogan PG, Kallies A, Lugli E, Lynn RC, Philip M, Rao A, Restifo NP, Schietinger A, Schumacher TN, Schwartzberg PL, Sharpe AH, Speiser DE, Wherry EJ, Youngblood BA, Zehn D. Defining "T cell exhaustion." Nat Rev Immunol. 2019;19(11):665–74. https://doi.org/10.1038/s41577-019-0221-9.
42. Addison EG, North J, Bakhsh I, Marden C, Haq S, Al-Sarraj S, Malayeri R, Wickremasinghe RG, Davies JK, Lowdell MW. Ligation of CD8alpha on human natural killer cells prevents activation-induced apoptosis and enhances cytolytic activity. Immunology. 2005;116(3):354–61. https://doi.org/10.1111/j.1365-2567.2005.02235.x.
43. Zambello R, Barilà G, Manni S, Piazza F, Semenzato G. NK cells and CD38: Implication for (Immuno)Therapy in Plasma Cell Dyscrasias. Cells. 2020;9(3):768. https://doi.org/10.3390/cells9030768.
44. Chen X, Li Y, Xia H, Chen YH. Monocytes in Tumorigenesis and Tumor Immunotherapy. Cells. 2023;12(13):1673. https://doi.org/10.3390/cells12131673.PMID:37443711;PMCID:PMC10340267.
45. Bronte V, Brandau S, Chen SH, Colombo MP, Frey AB, Greten TF, Mandruzzato S, Murray PJ, Ochoa A, Ostrand-Rosenberg S, Rodriguez PC, Sica A, Umansky V, Vonderheide RH, Gabrilovich DI. Recommendations for myeloid-derived suppressor cell nomenclature and characterization standards. Nat Commun. 2016;6(7):12150. https://doi.org/10.1038/ncomms12150.
46. Solito S, Marigo I, Pinton L, Damuzzo V, Mandruzzato S, Bronte V. Myeloid-derived suppressor cell heterogeneity in human cancers. Ann N Y Acad Sci. 2014;1319:47–65. https://doi.org/10.1111/nyas.12469.
47. Ren X, Tao Q, Wang H, Zhang Q, Zhou M, Liu L, Zhai Z. Monocytic Myeloid-Derived Suppressor Cells But Not Monocytes Predict Poor Prognosis of Acute Myeloid Leukemia. Turk J Haematol. 2022;39(4):230–6. https://doi.org/10.4274/tjh.galenos.2022.2022.0137.
48. Siemińska I, Węglarczyk K, Walczak M, Czerwińska A, Pach R, Rubinkiewicz M, Szczepanik A, Siedlar M, Baran J. Mo-MDSCs are pivotal players in colorectal cancer and may be associated with tumor recurrence after surgery. Transl Oncol. 2022;17:101346. https://doi.org/10.1016/j.tranon.2022.101346.
49. Yeap WH, Wong KL, Shimasaki N, Teo EC, Quek JK, Yong HX, Diong CP, Bertoletti A, Linn YC, Wong SC. CD16 is indispensable for antibody-dependent cellular cytotoxicity by human monocytes. Sci Rep. 2016;6:34310. https://doi.org/10.1038/srep34310.
50. Almeida J, Bueno C, Algueró MC, Sanchez ML, de Santiago M, Escribano L, Díaz-Agustín B, Vaquero JM, Laso FJ, San Miguel JF, Orfao A. Comparative analysis of the morphological, cytochemical, immunophenotypical, and functional characteristics of normal human peripheral blood lineage(-)/CD16(+)/HLA-DR(+)/CD14(-/lo) cells, CD14(+) monocytes, and CD16(-) dendritic cells. Clin Immunol. 2001Sep;100(3):325–38. https://doi.org/10.1006/clim.2001.5072.
51. Pittet MJ, Michielin O, Migliorini D. Clinical relevance of tumour-associated macrophages. Nat Rev Clin Oncol. 2022;19(6):402–421. https://doi.org/10.1038/s41571-022-00620-6. Epub 2022 Mar 30. Erratum in: Nat Rev Clin Oncol. 2022;19(6):424. https://doi.org/10.1038/s41571-022-00632-2.
52. Templeton AJ, McNamara MG, Šeruga B, Vera-Badillo FE, Aneja P, Ocaña A, Leibowitz-Amit R, Sonpavde G, Knox JJ, Tran B, Tannock IF, Amir E. Prognostic role of neutrophil-to-lymphocyte ratio in solid tumors: a systematic review and meta-analysis. J Natl Cancer Inst. 2014;106(6):dju124. https://doi.org/10.1093/jnci/dju124.
53. Szydełko J, Szydełko-Gorzkowicz M, Matyjaszek-matuszek B. Neutrophil-to-lymphocyte, platelet-to-lymphocyte ratios, and systemic immune-inflammation index as potential biomarkers of chronic inflammation in patients with newly diagnosed acromegaly: A single-centre study. J Clin Med. 2021;10(17).https://doi.org/10.3390/jcm10173997.
54. Allen BM, Hiam KJ, Burnett CE, Venida A, DeBarge R, Tenvooren I, Marquez DM, Cho NW, Carmi Y, Spitzer MH. Systemic dysfunction and plasticity of the immune macroenvironment in cancer models. Nat Med. 2020;26(7):1125–1134. https://doi.org/10.1038/s41591-020-0892-6. Epub 2020 May 25. Erratum in: Nat Med. 2024;30(5):1502. https://doi.org/10.1038/s41591-024-02947-2. PMID: 32451499; PMCID: PMC7384250.
55. Huang X, Xu J, Wu Y, Sheng L, Li Y, Zha B, Sun T, Yang J, Zang S, Liu J. Alterations in CD8+ Tregs, CD56+ Natural Killer Cells and IL-10 Are Associated With Invasiveness of Nonfunctioning Pituitary Adenomas (NFPAs). Pathol Oncol Res. 2021Mar;25(27): 598887. https://doi.org/10.3389/pore.2021.598887.
56. Ascierto ML, De Giorgi V, Liu Q, Bedognetti D, Spivey TL, Murtas D, Uccellini L, Ayotte BD, Stroncek DF, Chouchane L, Manjili MH, Wang E, Marincola FM. An immunologic portrait of cancer. J Transl Med. 2011Aug;29(9):146. https://doi.org/10.1186/1479-5876-9-146.
57. Melo V, Bremer E, Martin JD. Towards Immunotherapy-Induced Normalization of the Tumor Microenvironment. Front Cell Dev Biol. 2022May;30(10): 908389. https://doi.org/10.3389/fcell.2022.908389.

58. Fridman WH, Pagès F, Sautès-Fridman C, Galon J. The immune contexture in human tumours: impact on clinical outcome. Nat Rev Cancer. 2012Mar 15;12(4):298–306. https://doi.org/10.1038/nrc3245.
59. Sato M, Tamura R, Tamura H, Mase T, Kosugi K, Morimoto Y, Yoshida K, Toda M. Analysis of Tumor Angiogenesis and Immune Microenvironment in Non-Functional Pituitary Endocrine Tumors. J Clin Med. 2019May 16;8(5):695. https://doi.org/10.3390/jcm8050695.
60. He X, Xu C. PD-1: A Driver or Passenger of T Cell Exhaustion? Mol Cell. 2020Mar 5;77(5):930–1. https://doi.org/10.1016/j.molcel.2020.02.013.
61. Turchini J, Sioson L, Clarkson A, Sheen A, Gill AJ. PD-L1 Is Preferentially Expressed in PIT-1 Positive Pituitary Neuroendocrine Tumours. Endocr Pathol. 2021Sep;32(3):408–14. https://doi.org/10.1007/s12022-021-09673-2.
62. Wang PF, Wang TJ, Yang YK, Yao K, Li Z, Li YM, Yan CX. The expression profile of PD-L1 and CD8+ lymphocyte in pituitary adenomas indicating for immunotherapy. J Neurooncol. 2018Aug;139(1):89–95. https://doi.org/10.1007/s11060-018-2844-2.
63. Cai J, Wang D, Zhang G, Guo X. The Role Of PD-1/PD-L1 Axis In Treg Development And Function: Implications For Cancer Immunotherapy. Onco Targets Ther. 2019Oct;15(12):8437–45. https://doi.org/10.2147/OTT.S221340.
64. Takeuchi Y, Nishikawa H. Roles of regulatory T cells in cancer immunity. Int Immunol. 2016Aug;28(8):401–9. https://doi.org/10.1093/intimm/dxw025.
65. Francisco LM, Salinas VH, Brown KE, et al. PD-L1 regulates the development, maintenance, and function of induced regulatory T cells. J Exp Med. 2009;206(13):3015–29. https://doi.org/10.1084/jem.20090847.
66. Stathopoulou C, Gangaplara A, Mallett G, et al. PD-1 inhibitory receptor downregulates asparaginyl endopeptidase and maintains FoxP3 transcription factor stability in induced regulatory T cells. Immunity. 2018;49(2):247–263 e247. https://doi.org/10.1016/j.immuni.2018.05.006.
67. Zhang E, Ding C, Li S, Zhou X, Aikemu B, Fan X, Sun J, Zheng M, Yang X. Roles and mechanisms of tumour-infiltrating B cells in human cancer: a new force in immunotherapy. Biomark Res. 2023;11(1):28. https://doi.org/10.1186/s40364-023-00460-1.
68. Wu SY, Fu T, Jiang YZ, Shao ZM. Natural killer cells in cancer biology and therapy. Mol Cancer. 2020;19(1):120. https://doi.org/10.1186/s12943-020-01238-x.
69. Perri V, Gianchecchi E, Cifaldi L, Pellegrino M, Giorda E, Andreani M, Cappa M, Fierabracci A. Identification of GAD65 AA 114–122 reactive "memory-like" NK cells in newly diagnosed Type 1 diabetic patients by HLA-class I pentamers. PLoS ONE. 2017;12(12):e0189615. https://doi.org/10.1371/journal.pone.0189615.
70. Pal M, Schwab L, Yermakova A, Mace EM, Claus R, Krahl AC, Woiterski J, Hartwig UF, Orange JS, Handgretinger R, André MC. Tumor-priming converts NK cells to memory-like NK cells. Oncoimmunology. 2017Apr 18;6(6): e1317411. https://doi.org/10.1080/2162402X.2017.1317411.
71. Zaborowski MP, Stefens-Stawna P, Osztynowicz K, Piorunek T, Batura-Gabryel H, Dyzmann-Sroka A, Kozubski W, Nowak-Markwitz E, Michalak S. Granzyme B in peripheral blood mononuclear cells as a measure of cell-mediated immune response in paraneoplastic neurological syndromes and malignancy. Cancer Immunol Immunother. 2021;70(5):1277–89. https://doi.org/10.1007/s00262-020-02750-1.
72. Cheng X, Wang H, Wang Z, Zhu B, Long H. Tumor-associated myeloid cells in cancer immunotherapy. J Hematol Oncol. 2023;16(1):71. https://doi.org/10.1186/s13045-023-01473-x.
73. Ziegler-Heitbrock HW, Fingerle G, Ströbel M, Schraut W, Stelter F, Schütt C, Passlick B, Pforte A. The novel subset of CD14+/CD16+ blood monocytes exhibits features of tissue macrophages. Eur J Immunol. 1993;23(9):2053–8. https://doi.org/10.1002/eji.1830230902.
74. Zhou L, Wang M, Guo H, Hou J, Zhang Y, Li M, Wu X, Chen X, Wang L. Integrated Analysis Highlights the Immunosuppressive Role of TREM2+ Macrophages in Hepatocellular Carcinoma. Front Immunol. 2022;13:848367. https://doi.org/10.3389/fimmu.2022.848367.
75. Rőszer T. Understanding the Mysterious M2 Macrophage through Activation Markers and Effector Mechanisms. Mediators Inflamm. 2015;2015:816460. https://doi.org/10.1155/2015/816460.
76. Komohara Y, Ohnishi K, Kuratsu J, Takeya M. Possible involvement of the M2 anti-inflammatory macrophage phenotype in growth of human gliomas. J Pathol. 2008;216(1):15–24. https://doi.org/10.1002/path.2370.
77. Zhao Q, Huang L, Qin G, Qiao Y, Ren F, Shen C, Wang S, Liu S, Lian J, Wang D, Yu W, Zhang Y. Cancer-associated fibroblasts induce monocytic myeloid-derived suppressor cell generation via IL-6/exosomal miR-21-activated STAT3 signaling to promote cisplatin resistance in esophageal squamous cell carcinoma. Cancer Lett. 2021;518:35–48. https://doi.org/10.1016/j.canlet.2021.06.009.
78. Veglia F, Perego M, Gabrilovich D. Myeloid-derived suppressor cells coming of age. Nat Immunol. 2018;19(2):108–19. https://doi.org/10.1038/s41590-017-0022-x.
79. Caruntu A, Moraru L, Surcel M, Munteanu A, Costache DO, Tanase C, Constantin C, Scheau C, Neagu M, Caruntu C. Persistent Changes of Peripheral Blood Lymphocyte Subsets in Patients with Oral Squamous Cell Carcinoma. Healthcare (Basel). 2022;10(2):342. https://doi.org/10.3390/healthcare10020342.
80. Han C, Lin S, Lu X, Xue L, Wu ZB. Tumor-Associated Macrophages: New Horizons for Pituitary Adenoma Researches. Front Endocrinol (Lausanne). 2021;2(12): 785050. https://doi.org/10.3389/fendo.2021.785050.

Publisher's Note